INFORMATICS METHODS FOR ANALYSIS OF LUNG BRONCHOCONSTRICTION AND INFLAMMATION

by

ISRAR BIN MUHAMMAD IBRAHIM

(Under the Direction of RAMANA M PIDAPARTI)

ABSTRACT

Inflammation has been known to be the underlying cause of many diseases, including cancer, autoimmune conditions, atherosclerosis and infections, and is a major factor in aging. A well-known inflammation-associated disease in the lung is bronchoconstriction, which is commonly observed in asthma. Inflammatory diseases pose substantial global health and economic burden. Therefore, many experimental and computational studies have shed light on their dynamics and mechanisms. To further the understanding of inflammation dynamics, new methods are needed to complement experiments. The goal of this research is to develop informatics methods, including network and agent-based models, -to investigate inflammation dynamics and lung bronchoconstriction. Specific objectives of this dissertation include development of an informatics model of bronchoconstriction and agent-based inflammation, and development of new metrics to further analyze the underlying responses. The results of this study are consistent with the findings in the literature. Analysis of the results from information metrics indicated that bronchoconstriction is an adaptive network process and the network metrics can be used to identify its progression. Further, the course of inflammation and process of wound healing are related to the complexity of cell-to-cell interactions. These findings may help to further address the cellular level processes in various diseases and other applications.

INDEX WORDS: Lung, Inflammation, Informatics, Agent-Based Model, Graph Theory

INFORMATICS METHODS FOR ANALYSIS OF LUNG BRONCHOCONSTRICTION AND INFLAMMATION

by

ISRAR BIN MUHAMMAD IBRAHIM

BE, Syiah Kuala University, Indonesia, 2009

M.Sc, Virginia Commonwealth University, 2013

A Dissertation Submitted to the Graduate Faculty of The University of Georgia in Partial Fulfillment of the Requirements for the Degree

DOCTOR OF PHILOSOPHY

ATHENS, GEORGIA

2019

INFORMATICS METHODS FOR ANALYSIS OF LUNG BRONCHOCONSTRICTION AND INFLAMMATION

by

ISRAR BIN MUHAMMAD IBRAHIM

Major Professor: RAMANA PIDAPARTI
Committee: XIANQIAO WANG
K. MELISSA HALLOW
BENJAMIN DAVIS

Electronic Version Approved:

Suzanne Barbour
Dean of the Graduate School
The University of Georgia
August, 2019

DEDICATION

I dedicate this dissertation to my mother Husna, my father Muhammad Ibrahim and my family, Pante Geulima family.

Acknowledgments

Author (Israr) thanks Prof Ramana Pidaparti for his mentorship and guidance throughout all my Master and Ph.D. years. The author also thanks Dr. Xianqiao Wang for teaching him fundamentals of continuum mechanics, Dr. Benjamin Davis for teaching him fundamentals of multi-physics modeling, and Dr. K. Melissa Hallow for teaching mentorship and advise on the pharmacological aspect of the research. These contributions have helped to shape my research, this dissertation and my future research interests.

The authors thank the U. S. National Science Foundation for sponsoring the research through an NSF grant CMMI-1430379.

Author thanks all UGA College of Engineering colleagues, especially DICE LAB who have worked together since 2014. Special thanks to Parya Aghasafari, Kim Jongwon, and Sanjay Sharma O.V.

TABLE OF CONTENTS

Page

CHAPTER

LIST OF TABLES

Page

LIST OF FIGURES

Page

CHAPTER 1

INTRODUCTION

Inflammation is a response to stimulation by invading pathogens or endogenous signals such as damaged cells that results in tissue repair or pathology. For a long time, inflammation has been viewed as a beneficial response by the body to combat infections and recover injury. However, recent researches have shifted the perspective by revealing that inflammations, at times, can be harmful rather than beneficial, and a common factor in many diseases. Inflammation is initiated by complex interactions between cells, molecules, and pathways. The various pathways responsible for inflammation mean that inflammation can be switched on and off in any number of ways. Inflammation can lead to harmful consequences if it is initiated and is left active.

Inflammation has been known to be the underlying cause of many diseases, including cancer, autoimmune conditions, atherosclerosis and infections, and is a major factor in aging. In fact, there is an effort at unifying the principle of disease through inflammation [1][2]. The common theme in inflammation is the signaling of cells, release of cytokines and chemokines, destruction of cells such as epithelial cells, fibrosis, and resolution (wound healing, inflammation inhibition). Normally, once necessary conditions are fulfilled, the inflammation proceeds quickly, followed by gradual resolution. However, if mechanisms inhibiting inflammation are not present, then inflammation can persist at a low level (chronic inflammation). Resolution is not simply suppressing the stressing agent. The cells involved need to actively produce mediators to inhibit inflammation (homeostasis). Furthermore, the composition of the environment (the type of cells, the cytokines) and their interaction are important in determining the progression of inflammation and resolution [3].

The exact mechanism in which (chronic) inflammation causes various diseases to vary in terms of the cells involved is actively researched. For example, people who eventually develop diabetes have a high level of inflammatory molecules such as TNF-alpha. TNF-alpha may increase the production of glucose and triglycerides, which lower the performance of insulin in the absorption of blood sugar. Furthermore, insulin itself is anti-inflammatory. Hence, inflammation initiates the environment for insulin resistance that leads to (and even hastens) diabetes. The relation between cancer and inflammation can be straightforward. Inflammatory cytokines harm cells, damage the DNA, and create mutant genes that lead to cancer.

The lung tissue is in constant exposure to inflammatory agents such as pollutants and pathogens. These inflammatory agents can start or exacerbate bronchoconstriction such as asthma and chronic obstructive pulmonary disease (COPD). Another inflammatory disease in the lung is ventilator-induced lung injury (VILI) where inflammation is initiated by tissue overstretching.

Asthma and COPD are very common and their incidence is increasing globally, placing substantial health and economic burden [4]. Both diseases are characterized by airway constriction, ventilation heterogeneity (defects) and chronic inflammation markers. However, in some cases, the clinical features overlap, leading to difficulty in diagnosis. One defining characteristic distinguishing them is the distribution of the disease: asthma is mainly located in larger airways (conducting zone, although small airways can be affected too), while COPD predominantly affects small airways.

To understand the mechanism, the behavior, and to develop diagnostic measures, many experimental and computational models of inflammation have been developed and conducted. The dynamics of inflammation can be modeled using ordinary differential equation (ODE) of reaction-diffusion (RD) based models. For instance, inflammation was modeled as a consequence RD of cytokines [5] theorized to be involved in cell death. Cell death can then be obtained by solving a series of ODEs. A major shortcoming of the ODE-based model is that by ignoring spatial information, it may overlook important aspects of inflammation itself. The partial differential equation (PDE)-based model overcomes this limitation. However, this is not a popular approach in inflammation studies [6]. Some related studies used PDE-based models for understanding wound healing as a part of the mechano-sensitive response in tissue [7][8]. Another commonly employed approach in inflammation studies involves discrete-based models such as Cellular Automata (CA) [9]. The discrete model has an advantage in that it accounts for both spatial and temporal aspects as well as stochasticity.

Several studies have demonstrated the feasibility of using a discrete model to explain aspects of acute pulmonary inflammation. For instance, Angela et al. used a CA model to study bacterial infection and healing in a model lung environment [10]. Another model used the discrete model to study inflammation induced by particulate matter inhaled into the lung [11]. Other applications of CA models include cancer spread modeling [12][13], disease infection [14] and inflammation [10][11][15]. However, this study did not address the effect of agent interactions in inflammation progression and resolution.

On the other hand, studies of the lung ranging from acoustic analysis [16], tissue deformation [17] and fluid analysis [18] have been carried out. However, bronchoconstriction involves interaction between millions of airway at different hierarchical sites. There is a lack of investigations into the behavior of airways interaction and the morphological changes it induces.

1.1 KNOWLEDGE GAP

Several studies have demonstrated the feasibility of using a discrete model to explain aspects of acute pulmonary inflammation. For instance, Angela et al used a CA model to study bacterial infection and healing in a model lung environment [10]. Another model used the discrete model to study inflammation induced by particulate matter inhaled into the lung [11]. However, these models did not incorporate the effect of mechanical strain in inflammation.

Recently, there is a growing interests in applying information theoretic approach for analysis of physical and biological system [19] [20]. This is based on the premise that information is physical and may govern or drive physical systems. Using this approach, biochemical reactions can be formulated as a process that converts information into work [21]. Cells migration and inflammation are dependent on signal transduction and certain series of events. An impairment in cell communication leads to all sorts of disorders and diseases. However, there is a lack of study and framework for inflammation in terms of information as a quantity. By quantifying information, it is possible to quantify cell-to-cell and cell-to-environment interactions and it may help explain why certain chain of events lead to either normal or chronic inflammations.

Another application of information theoretic approach is the use of mathematical graph (or network) as domain of a model (instead of Euclidian space). The graph analog of PDE has been proposed by Ref [22]. Some problems can be naturally formalized using graph domain, such as leaf venation formation [23], river network structure and its effect on ecological biodiversity [24], and spatial evolution of cities [25]. This formulation enable investigation into factors that drive their morphological evolutions. However, there is a lack of graph-based formulation of lung dynamics.

1.2 DISSERTATION OVERVIEW AND RESEARCH OBJECTIVE

The rest of this dissertation is divided into three chapters. Chapter 2 presents the agent-based model for inflammation. Chapter 3 presents the informatics analysis of inflammation, and Chapter 4 presents a network model for lung bronchoconstriction. Fig 1.1 illustrates the work flow of this research.

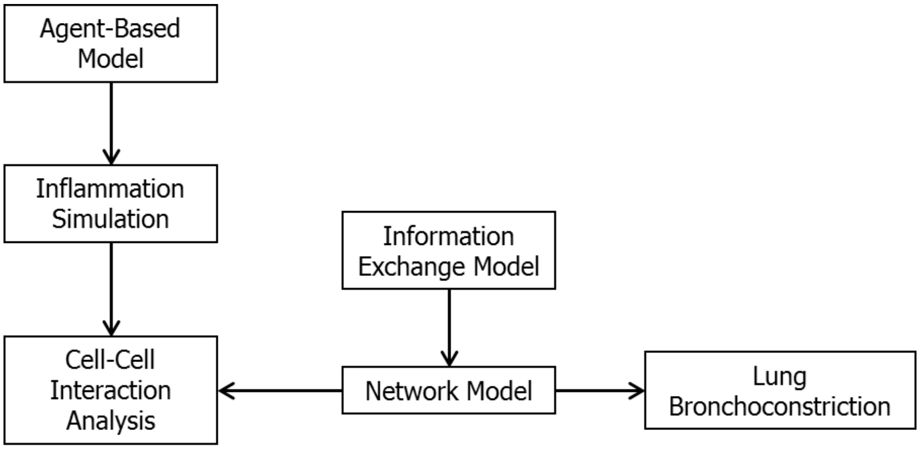

Figure 1.1. The models developed in this research and their applications.

The objective of this research is to develop informatics methods to fill the knowledge gaps mentioned previously. Informatics methods consist of a number of tools to properly describe and investigate the interaction between many components in a system. Informatics attempts to implement concepts from information theory for problems in various fields such as biology, physics, and health science. Methods and concepts employed in informatics include agent-based model, network theory and its complexity measures, and information flow/exchange. Specifically, the objective of this research is,

1) Development of an informatics model of bronchoconstriction as a tool to investigate the relationship between lung structural complexity and disease progression.
2) Development of an agent-based model for inflammation to carry out analysis of inflammation in terms of cells interactions and collective dynamics.
3) Development of informatics model to identify dominant factors in the complex interrelationship of agents in the inflammation process.

This research is conducted based on the following hypotheses:

1) The course of inflammation can be modulated by mechanical stimuli
2) Flow of information (among cells, between cells and environment) plays an important role in determining the outcome of inflammation.
3) Bronchoconstriction is similar to network optimization process that removes edges to optimize the current state of the network.

CHAPTER 2

SIMULATION OF WOUND HEALING AND CELL'S DYNAMICS UNDER STRAIN-INDUCED INFLAMMATION

2.1 INTRODUCTION

Acute lung injury (ALI), acute respiratory distress syndrome (ARDS), and chronic obstructive pulmonary disease (COPD) cause significant inflammation, especially in patients who are subject to mechanical ventilation. Despite the well-known ventilation-associated inflammation and organ failure risks [26], mechanical ventilation is still an essential approach for restoring respiratory function in patients. The main risk with mechanical ventilation is that it leads to excessive pressure, which induces mechano-sensitive pathways in alveolar tissue that may lead to inflammation as well as systemic organ failure. Inflammation can be characterized as a complex chain reaction involving tissue constituents along with many cytokines and leads to tissue damage that reduces the functionality of organs. For instance, stretch-induced inflammation is known to cause a cascade of organ failures during mechanical ventilation.

In this study, we simulated a virtual lung environment to study the influence of the elastic field on the dynamics of inflammation. The elastic field is a term borrowed from solid mechanics to describe strain or stretch. This elastic field is seen as a potential factor that drives the tissue constituents to inflammation states. A discrete informatics model that accounts for probabilistic adaptation using existing experimental data was developed. The model is largely discrete to conform to the CA model paradigm and is built upon a mechanistic approach to each tissue constituent in the inflammation process. The model developed here reflects the redundant chain of events and shows certain thresholds of tissue recovery during inflammation. Several scenarios of strain levels are investigated and the results obtained are presented and discussed.

2.2 CELLULAR AUTOMATA

CA is a discrete and rule-based model that has been used for both physics and biological modeling. A well-known compilation of CA-oriented physical model is a work by Chopard and Droz [9]. They covered common physical model such as fluid flow, elastic solid, diffusion and reaction-diffusion. Ermentrout et al [12], compiled various CA model in biology. This works covered CA model built to give pattern commonly found in biological system. The models built based on description of the components and interactions in associated biological system. Recent application of CA includes cancer spread modeling [13], disease infection [14] and inflammation [10]. These models consist of several "agents" that interacts to give rise to the dynamics of the environment. Reynolds et al [10], defined several agents in the model that represent epithelium and macrophages with finite states. These agents change states according to environmental interactions. Other studies would provide further information on possible agents definition on CA model [11][15].

A CA model typically consists of a set of uniform "cells" (or agents), space represented by grids, and rules that define the cells behavior. The cells can be seen as mini-computer that computes the rules. Mathematically, a CA is defined in terms of set theory as a tuple:

$$\mathrm{A} = \{\mathrm{G}, \mathrm{E}, \mathrm{U}, \mathrm{f}\} \tag{2.1}$$

where G , E , U and f are a grid of cells, set of finite states of cells, set of neighborhood and set of local rule, respectively. The grid is typically defined as d-dimensional square grid, that is $\mathrm{G} = \mathbb{Z}^{\mathrm{d}}$. The state is typically defined as a finite set of numbers (e.g., binary, real). There is various definition of neighborhood, one of the most used is Moore's neighborhood, defined as $\mathrm{U}(\mathrm{x_i}) = \{\mathrm{x} | \|\mathrm{x_i} - \mathrm{x}\|_\infty \le 1\}$. The local rule defines the evolution of state. The general form of rule is,

$$\mathrm{z(x)^{t+1}} = \mathrm{f}\left(\mathrm{z^t}|_{\mathrm{U(x)}}\right) \tag{2.2}$$

where $\mathrm{z(x)^t}$ is state at x at time step t, and $\mathrm{z^t}|_{\mathrm{U(x)}}$ is state at the neighborhood of x. One of the most common forms of local rules in CA is employing conditionals, which can also be represented as step function,

$$\mathrm{z^t} \begin{cases} 1 & \text{if A} \\ 0 & \text{else} \end{cases} \tag{2.3}$$

where A is conditional statement(s). The conditional statements typically involve the states of neighbors. Other recurring local rule is the summation of states,

$$\mathrm{z(x)^{t+1}} = \mathrm{z(x)^t} + \sum \mathrm{z^t}|_{U(x)} \tag{2.4}$$

In this study, these two general forms of rule are used. The boundary of CA grid can be defined by two conditions: fixed or periodic. Fixed boundary condition imposes a constant value on the boundary. Periodic boundary lends itself from molecular modeling, and is used to approach large domain. It imposes continuum between two opposite facing boundaries. This condition can also be seen as a domain which satisfies torus topology.

2.3 DETAILS ON AGENT-BASED MODEL FOR INFLAMMATION

Inflammation is a complex process that involves the release and spread of cytokines and cell's interaction with the environment. Inflammation is mainly the interplay between reaction-diffusion (R/D) of cytokines and cells response. To model this, discrete computational method was employed. The model is based on CA. The discrete model employed in this study is largely based on probability. As usual, the CA model is built upon a definition of grid. In this study, square two-dimensional grid is used. There are four layers of grid: epithelial cells, motile cells (cells with motility), cytokines, proteins and elastic field grid. As per CA modeling, the evolution of the grids is dictated by a set of rules. The rules and grids are explained below. Fig 2.1 illustrates the CA model with multiple grids, as well as a graph showing the causal path of the CA model.

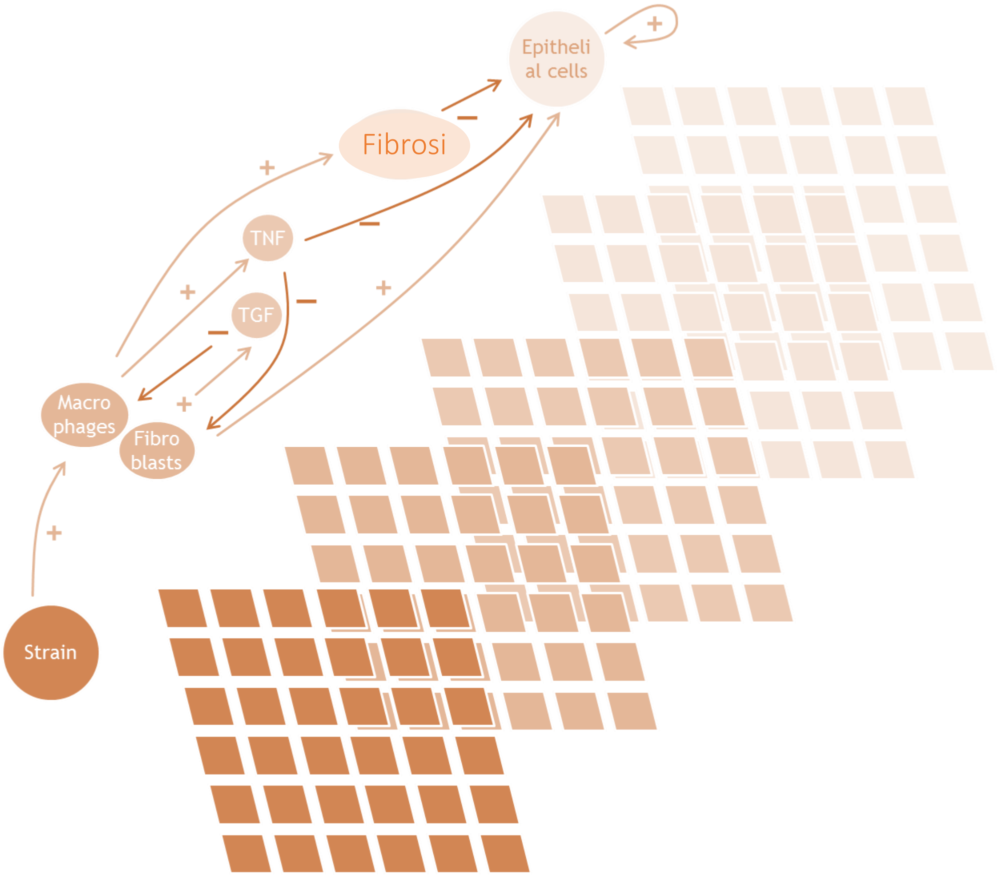

Figure 2.1: CA with multiple grids, each grid represents the event and dynamics in the tissue. The graph on the left shows the causal path of the events. Each edge associated with plus (+) sign represent positive feedback to the vertex it is pointing on (activation, release/adding concentration, healing), while the one associated with negative sign (-) carries negative feedback (inhibition, damage).

2.3.1 EPITHELIAL CELLS GRID

The epithelial cells grid is a typical CA grid, with only two states: 1 and 0, representing “dead” and “healthy”, consecutively. The rules that defines evolution of the CA cells in this grid are,

$$z_1^{t+1}(x) = \begin{cases} 1, & rand(\alpha_1, \beta_1) < z_{3TNF}^t(x) \\ 0, & otherwise,\ or\ healing \end{cases} \quad (2.5)$$

$$z_1^{t+1}(x) = samp(d, w) \quad (2.6)$$

where $z_1^t(x)$ is the epithelial cell's state at time step t and location x, $z_{3TNF}^t(x)$ is concentration of pro-inflammatory cytokine occupying the same grid coordinate, $rand$ is random number generator based on beta function probability density, α_1 and β_1 are two beta function parameters, and $samp(d, w)$ is random sampling algorithm that samples data set d by weights w. Eq. 2.5 describes the state transition by cytokine and fibroblast. The healing condition comes from cell mitosis and fibroblast, and described by Eq. 2.7 and 2.8 below,

$$unirand < P_{mt} \quad (2.7)$$

$$z_1^{t+t_h}(x) = 1 \quad when\ z_{2f}^t(x) = 2 \quad (2.8)$$

where $unirand$ is uniform random number generator between 0 and 1, P_{mt} is mitosis rate, and z_{2f}^t is the state of motile cells grid. The mitosis rate defines the probabilistic rate of mitosis, as part of self-healing process of the cells. Eq. 2.6 describes state transition by the presence of fibrosis (explained in Fibrosis section). Function $samp$ randomly chooses the state of a cell, d, with some bias w. In this case, d is the possible state the grid can have (i.e., 0 and 1). The weight w skews $samp$ to choose state 1 according to the numbers of fibrosis site at vicinity (*Nc*). The rationale for damage caused by fibrosis is that the more fibrosis occurs in a location, the more likely it is to cause damage to tissue.

2.3.2 MOTILE CELLS

The motile cells are capable to move according to concentration gradient (chemotaxis). The grids can contain three states: 0, 1, and 2, representing non-existence of cells, inactivated, activated and secondary state for the motile cells. Simple probabilistic model of cell motility is used here, i.e.,

$$a_2 = samp(U(x,r),\ z_3^t(x)) \tag{2.9}$$

$$z_2^{t+1}(x)|_{U(x)} = \begin{cases} 1, & at\ z_2^t(a_2) \\ 0, & otherwise \end{cases} \tag{2.10}$$

where $samp(w,d)$ has been used once again, with different terms regarding w and d. In this case, $samp$ randomly choose local grid site according to neighborhood $U(x,r)$ where r is neighborhood radius, and the choice is biased according to z_3^t, which is the state of cytokine grid at current cell location, x. Variables in Eq. 2.10 is as follow: $U(x)$ is Moore's neighborhood function, $z_2^t(x)$ is the state of motile cell's grid at time step t.

There are two type of motile cells, the macrophages (agent of inflammation) and fibroblasts (agent of healing). The state transition of the grid is applied toward grid with state $z_2^t(x) > 0$ (the grid occupied by motile cells), and governed by rule as follow,

$$z_2^{t+1}(x) = \begin{cases} 1 & t_{pop} > \epsilon_{pop} \\ 2 & z_1^t = 1\ (fibroblast), rand(\alpha_2, \beta_2) < z_4^t(x)(macrophage) \\ 0 & otherwise\ or\ if\ t_{im} > \epsilon_{im} \end{cases} \tag{2.11}$$

where ϵ_{im} is the age of motile cells, $z_4^t(x)$ is the state of elastic field grid (which will be explained later) and the random number generation using beta function probability density has been used once again. The rule in Eq. 2.11 is applied to both type of motile cells, only differ in minor detail as follow (including the rule for activation as shown in Eq. 2.11). The macrophages are still mobile after activation, while fibroblast will stay at the last grid site after activation. The latter represents fibroblast healing at injured site. This means the rule in Eq. 2.9 and 2.10 still applies to macrophages after activation, but not fibroblasts. In addition, the ϵ_{im} of fibroblast also reduced by 75% after activation.

When activated, the motile cells release cytokines. Each type of motile cells is associated with specific cytokine (i.e., macrophage releases TNF, and fibroblast release TGF). Macrophage tends to release TNF where the environment experiences more strain, while fibroblast tends to release TGF in presence of TNF. However, TGF inhibits macrophage in releasing TNF. Hence, the CA reflects activator-inhibitor system. The cytokines release by motile cells can generally be expressed as,

$$z_{3TNF}^{t+1}(x) = \begin{cases} 1, & rand(\alpha_3, \beta_3) \geq z_{3TGF}^{t}(x) \; when \; z_{2m}^{t}(x) = 2 \\ 0, & otherwise \end{cases} \tag{2.12}$$

$$z_{3TGF}^{t+1}(x) = \begin{cases} 1, & rand(\alpha_4, \beta_4) \leq z_{3TNF}^{t}(x) \; when \; z_{2f}^{t}(x) = 1 \\ 0, & otherwise \end{cases} \tag{2.13}$$

where $z_3^t(x)$ is the state of cytokine grid at time t, the subscript denotes the type of cytokine, $z_2^t(x)$ is the state of motile cell grid at the same time step, and subscript m and f denote the type of motile cell which is macrophage and fibroblast, consecutively, α and β are beta function parameters which are given in Table 2.1. Fig 2.2 illustrates the beta probability distribution that describe relations in Table 2.1.

Table 2.1: Beta Function Parameters

No	Case	α	β
1	Epithelial cells grid (Eq A5)	5	1
2	Macrophages activation (Eq A11)	5	1
3	TNF Release (Eq. A12)	1	3
4	TGF Release (Eq. A13)	2	1

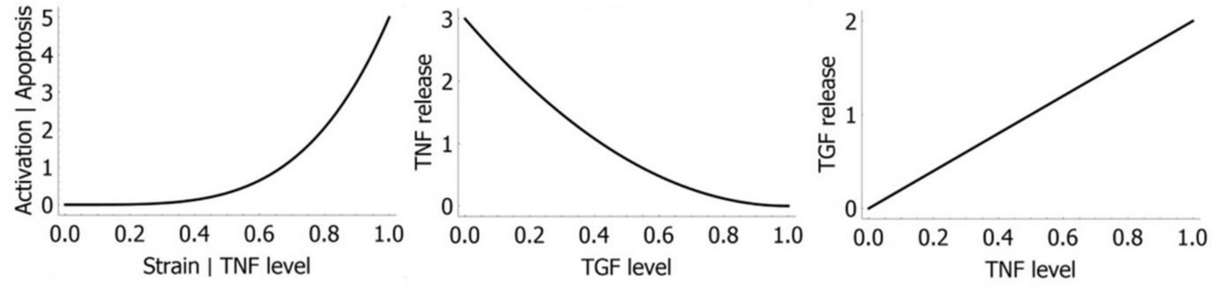

Figure 2.2: Illustration of beta distribution that determine probabilistic relations in Table 2.1 and Table 2.3.

The population of motile cells are also kept at averagely n_{im} numbers, with 0.25 variance. This means the top condition in Eq. 2.11 applies at random grid location to ensure the population is at n_{im} on average. As before, the beta function and rules parameters are given in Table 2.1 and Table 2.2, consecutively.

Table 2.2: Model parameters for simulations

Mitosis probability, P_{mt}	1/5
Healing time, t_h	5

Fibrosis time, K_c	0.1
TNF diffusity, D	0.07
TGF diffusity, D	0.1
TNF dissolution constant, K	1×10^{-3}
TGF dissolution constant, K	1×10^{-5}
Collagen damage probability	$Nc/9$
Repopulation of motile cells, ϵ_{pop}	5 iterations
Motile cells life time, t_{im}	20 iterations
Motile cells velocity ($\propto r$)	3 cells/ iterations
Population of motile cells	25

2.3.3 CYTOKINE GRID

The cytokine grid contains an array of CA cells to simulate the spread of cytokines by diffusion, and its disintegration over time. One way to simulate spread is to employ additive rule such as,

$$z_3(x)^{t+1} = \sum_{U(x)} k_i \, z_3(x)^t \tag{2.14}$$

where k_i is a set of constant corresponding to neighborhood function, $U(x)$. To determine k_i, one may gain insights from a system appear as numerical solution of diffusion equation with additional disintegration terms,

$$dC/dt = D \cdot \nabla^2 C - K \cdot C \tag{2.15}$$

where C is concentration, D is diffusity, K is a constant determining the rate of disintegration. Numerical solution by Finite Difference Method gives,

$$z_3^{t+1}(x) = z_3^t(x) + D \sum_{U(x)} k_i \, z_3^t(x) - K \, z_3^t(x) \tag{2.16}$$

where Neumann's neighborhood is used, and cells have continuous state, and $k_i = 1 - 4D$ for $U(x) = 0$, and $k_i = D$ otherwise. Values of D and K are shown in Table 2.1.

2.3.4 ELASTIC FIELD GRID

It is theorized that mechanical strain on tissue activate ion channel(s) on the cells that leads to the release of array of cytokines [27]. In this model, the mechanical strain is represented by another layer of CA grid as a discretized strain field. The FEM simulation in the study provide insights of the strain distribution. This is translated into discretized distribution of strain field in the CA grid. This strain field acts energy gradient in activating the motile cells. The model simplifies the activation process by ignoring molecular mechanism of ion channels opening by strain and cells signaling pathway that leads to release of specific cytokines. In addition, only macrophage is activated by strain. The rule dictating macrophage activation is expressed in Eq. 2.10.

2.3.5 FIBROSIS

The healing by fibroblasts release TGF that contributes to production of collagen. Hence, there is a surge of collagen concentration as a result of healing by fibroblasts. This introduces scar to the tissue, and reduce tissue compliance. In the present study, we represent this phenomenology where collagen deposits produced after healing add risks to damage on epithelial cells. In CA, the site of these collagen deposits are the same as the location of fibroblast after activation. The effect of these collagen deposits will stay after specified time, as shown Table 2.2 as fibrosis time. The rule of collagen deposits is as follow,

$$z_5^{t+t_h}(x) = \begin{cases} 1, & at\ z_{2f}^t(x) = 2 \\ 0, & otherwise \end{cases} \tag{2.17}$$

2.3.6 SUMMARY OF RULES

To summarize the CA rules, Table 2.3 outlines the rules according to the grid types. These rules were implemented in MATLAB. The statistical toolbox has been used for random algorithm $rand$ and $samp$. The $samp$ is basically a randomized data sampling algorithm, and Matlab R2016 uses the algorithm by Wong and Easton [28].

The simulation is run for a domain representing tissue experiencing mechanical strain, expressed in elastic field grid of CA. The grids contain 100 by 100 cells, where a biological epithelial cell size is around 1 μm. The boundary condition used is periodic boundary condition, where continuum between two opposite edge of the boundary is imposed, that is,

$$z^t|_{\Gamma_1(x)} = z^t|_{\Gamma_2(x)} \tag{2.18}$$

where Γ_1 and Γ_2 are set of two opposing boundaries.

Table 2.3: Summary of CA model developed for this study. The state value 0 and 1 for list No.1 mean dead and living. The state value 0, 1 and 2 of grid No.2 are: inactivated, activated and empty grid. The state value of grid No. 3 and 4 represents concentration of associated. z_i^t is state of grid, where i is subscript that refers to number assigned for each type of grid (column 1).

No	Type	Behavior	Rules
1	Epithelial cells	Fixed	**State transition**: Apoptosis is highly likely as TNF increases [29] $z_1^{t+1}(x) = \begin{cases} 1, & rand(\alpha_1, \beta_1) < z_{3TNF}^t(x), or \\ 0, & otherwise,\ or\ \textbf{healing} \end{cases}$ $z_1^{t+1}(x) = samp(d, w)$ **Healing**: 1. Mitosis: $unirand(0,1) < P_{mt}$ 2. Fibroblast: $z_1^{t+t_h}(x) = 1\ when\ z_{2f}^t(x) = 2$
2	Motile cells	Mobile	**Locomotion**: Motile cells move by biochemical gradient [30] $a_2 = samp(U(x, r), z_3^t(x))$ $z_2^{t+1}(x)\|_{U(x)} = \begin{cases} 1, & at\ z_2^t(a_2) \\ 0, & otherwise \end{cases}$

			Repopulation: $x = (n_{grid})\ unirand(0,1)$ $z_2^{t+t_{pop}}(x) = 1$
	Macrophage		**State transition**: Macrophage is activated by TNF, and releases TNF where strain level is high [31][32] $z_{2m}^{t+1}(x) = \begin{cases} 1 & t_{pop} > \epsilon_{pop} \\ 2 & rand(\alpha_2,\beta_2) < z_4^t(x) \\ 0 & otherwise\ or\ if\ t_{im} > \epsilon_{im} \end{cases}$ **TNF release**: $z_{3TNF}^{t+1}(x)$ $= \begin{cases} 1, & rand(\alpha_3,\beta_3) \geq z_{3TGF}^t(x)\ when\ z_{2m}^t(x) = 2 \\ 0, & otherwise \end{cases}$
	Fibroblast		**State transition**: Fibroblast is likely to release TGF in the presence of TNF [33]. It is activated by the presence of dead epithelial cell, and will differentiate at the location of damage. TGF increases collagen synthesis [34] $z_{2f}^{t+1}(x) = \begin{cases} 1 & t_{pop} > \epsilon_{pop} \\ 2 & z_1^t = 1 \\ 0 & otherwise\ or\ if\ t_{im} > \epsilon_{im} \end{cases}$

			TGF release: $z_{3TGF}^{t+1}(x)$ $= \begin{cases} 1, & rand(\alpha_4, \beta_4) \leq z_{3TNF}^{t}(x) \; when \; z_{2f}^{t}(x) = 1 \\ 0, & otherwise \end{cases}$ **Fibrosis Location**: $z_5^{t+t_h}(x) = \begin{cases} 1, & at \; z_{2f}^{t}(x) = 2 \\ 0, & otherwise \end{cases}$
3	Cytokines	Diffusing	**State Transition** (Diffusion, continuous value): Diffuse and disintegrate [30] $z_3^{t+1}(x) = z_3^t(x) + D \sum_{U(x)} k_i \, z_3^t(x) - K \, z_3^t(x)$
4	Elastic Field	Constant	**Constant States**
5	Fibrosis		**Decaying**: $z_5^{t+1} = K_c * z_5^t$

2.4 SHANNON'S ENTROPY

Shannon's entropy is a measure of information content in a sequence or in a data. It is expressed as,

$$S = -\sum_i P_i \log_2 P_i \tag{2.19}$$

where S is Shannon's entropy, and P_i is the sequence or data. A homogeneous sequence (such as {0,0,0,0}) has zero entropy. Shannon's entropy can be used to quantify the order of a configuration in two-dimensional space. Disordered configuration has higher Shannon's entropy than uniform configuration.

2.5 IMPLEMENTATION

The model is implemented using MATLAB R2016A. The code was designed to be modular. Several modules were categorized in the implementation: cells life cycle module, cell motility, cell population, and the diffusion module. The cells life cycle module controls the changes in cells’ states during the simulation. The cells motility module controls the dynamics of the cells’ taxis while the cell population module regulates cells’ population during the simulation and initial cells’ placement. Finally, the diffusion module generates the spread of cytokines through diffusion. All modules except the diffusion module are designed to be probabilistic. The MATLAB random generation function included in Statistical Toolbox was used.

Using the code developed, several cases were simulated. These case studies were also used to test the validity of our model. Additional details on the case studies are presented in the next section. The grid for all cases was defined as a square grid and periodic boundary conditions were applied. Each cell represents the scale size of a cell (approximately 1 μm).

The CA model is a qualitative model; hence, it did not use real values (with units). The states of CA cells representing physical variables (strain and cytokines concentration) were expressed as continuous values between zero and one. This can be interpreted for analysis using normalized values, or as a state between non-existent strain or cytokines, and maximum strain or cytokines on a discrete location.

The model consists of several parameters (as listed in Table 2.1 and Table 2.2 for the case). It is difficult to determine these parameters, but some justifications and assumptions can be made. The use of distribution function can be inferred from experiments that measure the dependency of events in inflammation. For example, beta distribution parameters were inferred from results in

[32]. Other beta distribution parameters were assumed to follow the results in [32], with a slight modification to increase or reduce its occurrence. These parameters were selected from numerical experiments and used throughout the case studies.

The assumption for other parameters in Table 2.2 is as follows. Constants D and K can be inferred from the behavior of the activator-inhibitor system. The activator typically diffuses faster and does not remain longer than the inhibitor, hence $D_{TNF} > D_{TGF}$ and $K_{TNF} > K_{TGF}$. Next, we assumed the fibrosis is a byproduct of healing (by fibroblasts) and remains longer than the process of healing itself. Results from a previous study [11] also helped to determine the values of motile cells population and velocity.

The code was run in a workstation with the following specifications: Windows 7 Operating (64 bit) system, 2.6 GHz processor (Intel Xeon) and 64 GB RAM. MATLAB parallel processing was not implemented into the code. We carried out ten simulations for each of the cases considered below. Each case was run for 10,000 iterations.

2.6 RESULTS

The CA model grid represents tissue under mechanical stress. Three levels of tissue strain, low (0.35), medium (0.5) and high (0.9) were considered. These magnitudes of strain may be related to physiological relevant cases for smaller airways under different mechanical ventilation conditions (low/high tidal volume and PEEP) [35]. The CA model is used to quantify the population dynamics of the cells, which can be used to infer the severity of inflammation. The results of inflammation obtained from the simulations are presented below.

2.6.1 QUALITATIVE VALIDATION

Fig 2.3 shows the time course of simulation in terms of the number of dead epithelial cells (top left), also termed as inflammation score. The result shows a typical inflammation time course, as described in Refs. [34][36][37]. The time course generally consists of inflammation phase and recovery (wound healing) phase and can be identified by the fluctuation of the number of cells involved in the process.

Fig 2.3 also shows spatial visualization of cells (top right) of the simulation after iteration 500, which depicts multiple injury sites (grey regions), including two marked locations (A and B) where most motile cells congregated. The next two plots below it show the number of macrophages and fibroblasts on location A and location B during the simulation time course. It can be seen that the elevation of injury was followed by an increased number of macrophages. This is eventually followed by a recovery phase where fibroblasts migrated (the number of fibroblast on each location increased) and repaired tissue (the number of dead epithelial cells decreased). These results demonstrate that the model is capable of replicating events commonly found during inflammation, as described in various literature [34][36][37].

In Fig 2.3, we can also observe that the number of iterations for the simulation to complete (i.e., simulation time) to exhibit inflammation and healing phase is 10,000 iterations. If we consider the velocity of motile cells, V_m to be in the range of 1 to 10 microns/min [38] (where motile cells migrate at each iteration), and a grid size to be in the range of 10-20 microns (corresponds to the size estimate of macrophage and fibroblast [39][40], then the total simulation time can be estimated to be $10000 \times V_m$, which corresponds to 10,000 to 100,000 minutes or approximately 7 to 70 days.

These values are within the range of actual wound healing time span as reported in literatures such as [41].

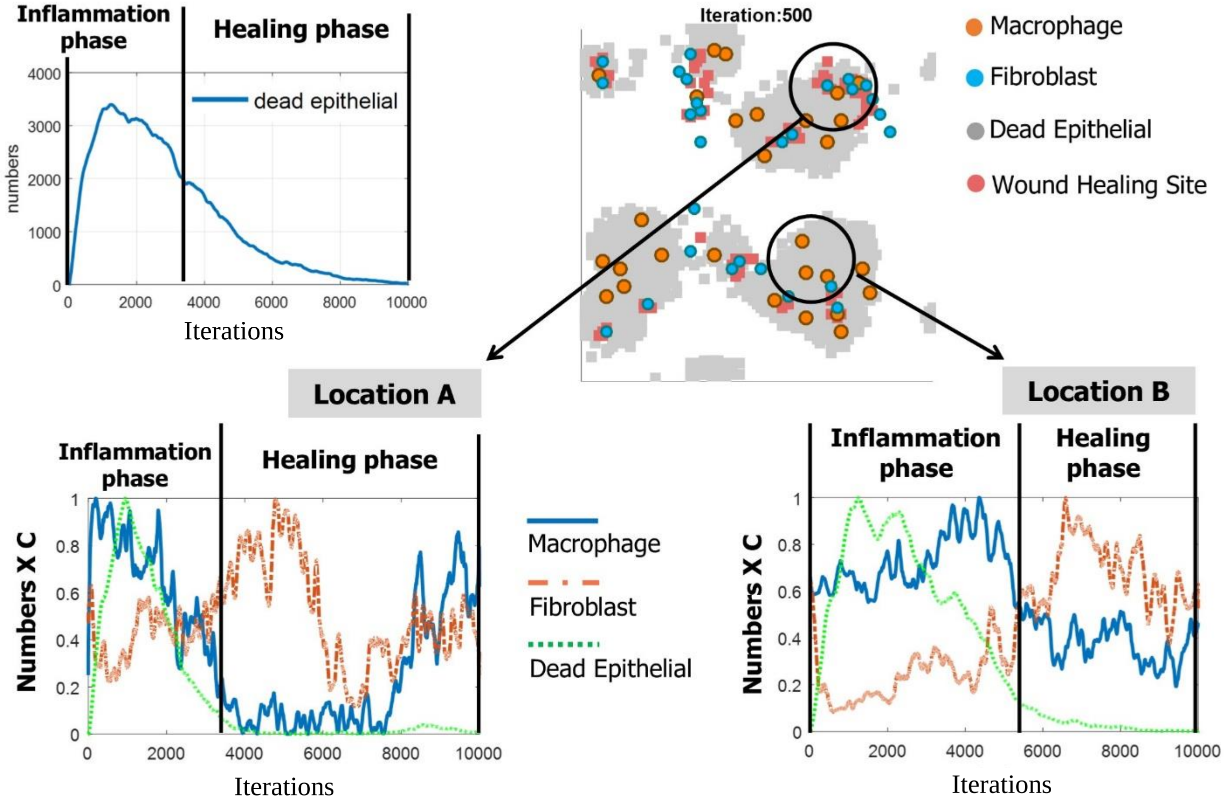

Figure 2.3: A sample of inflammation time course. Top left: time course dead epithelial cells (injury severity) on the whole tissue space, depicts phase of elevated injury (number of death of epithelial cells) followed by recovery. Top right: visualization of spatial aspects of the model, showing the location of injury (dead epithelial cells), macrophages, fibroblasts and wound healing site. Middle and Bottom: number of macrophages, fibroblasts, and dead epithelial cells on Location A and Location B.

2.6.1.1 PRO- AND ANTI- INFLAMMATORY CYTOKINES

The pro-inflammatory cytokines and anti-inflammatory cytokines exhibit the natural process of the activator-inhibitor system [42]. In this model, as activated motile cells move, they release cytokines. One defining feature of the activator-inhibitor system is that in the presence of anti-inflammatory cytokines, pro-inflammatory cytokines will be suppressed. To demonstrate this behavior in this model, we took a sample (10 samples) of results with a strain=0.35. This is shown in Fig. 2.4 and 2.5. Fig. 2.4 shows the state of two cytokines at 400 iterations. Fig. 2.4(a) shows the CA grid of TGF. Fig. 2.4(b) is the CA grid of TNF.

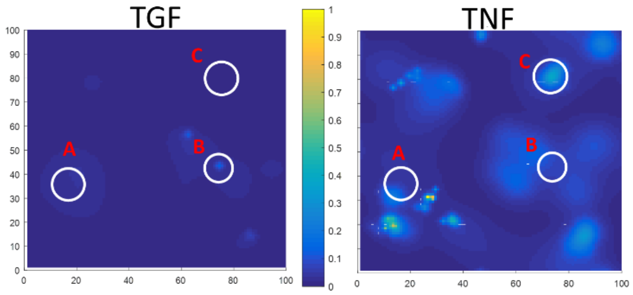

Figure 2.4: (a) the state of TGF cytokines on the grid, (b) the state of TNF cytokines. Both were at t=400. The color plots represent the state (concentration) of TGF and TNF.

As can be seen in Fig. 2.4(b), TNF at Location A and B had spread, and it triggered the release of TGF at these two locations as well (as can be seen in Fig. 2.4 (a)). Fig 2.5 shows the time course in these two locations. As can be seen, as TNF concentration at A (circle-blue lines) diffused, it triggered the release of TGF at A (dotted-circle red lines) at around 200 simulation time. Afterward, the TGF concentration rose and suppressed the concentration of TNF (as can be seen in declining circle-blue lines at approximately 300 simulation time).

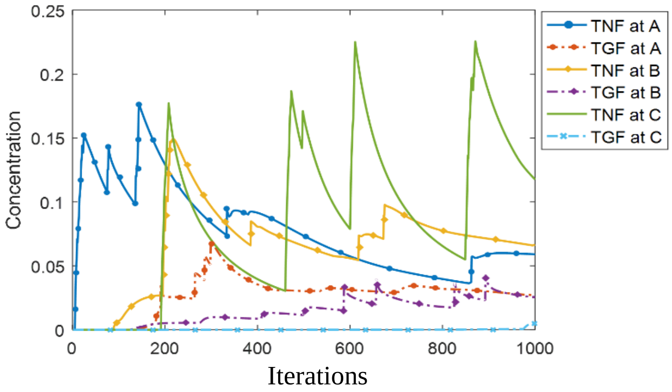

Figure 2.5: The behavior of TNF and TGF resembles an activator-inhibitor system. The letters correspond to locations indicated in Fig 2.4.

The same behavior can be seen for Location B (diamond-yellow and diamond-dotted purple lines). As TGF concentration increased over time (diamond-dotted purple lines), the TNF concentration (diamond-yellow lines) declined. On the other hand, when an anti-inflammatory cytokine is not present, the pro-inflammatory cytokine maintains its presence. This is demonstrated in Location C. As can be seen in Fig. 2.4 (b), there was the presence of TNF at C, but the location was lacking TGF (Fig. 2.4 (b)). Hence, as can be seen in Fig. 2.5 (green line), the TNF kept releasing (the spike) and diffused at the location, while TGF was non-existent.

Thus, it has been demonstrated that the activator-inhibitor system exists on the CA grid, although there is no explicit coupling between the two cytokines in the model. The activator-inhibitor system portrayed by motile CA cells' (stochastic) movement and cytokines diffusion keeps signaling the motile CA cells. We only presented one sample result in this subsection since the results presented so far are specific to a location. The release of cytokines is random; therefore, in the other sample results, the locations of release will be different from the ones shown in A, B, and C. However, one can infer the consistency of this model's stochastic simulation from the overall behavior of the informatics model, which is discussed in the subsection below.

2.6.2 SENSITIVITY ANALYSIS

Sensitivity analysis was carried out by running simulations with the same parameters (as listed in Table 2.1 and 2.2) ten times. These parameters determine a case (such as chronic or normal inflammation case), therefore they are fixed variables for sensitivity analysis. When a simulation is initialized, the locations of motile cells are randomized. Then the events are executed according to probability rules. To test sensitivity of the model to initial conditions, ten simulation trials were carried out. Fig 2.6 (a) shows all results of ten simulation trials plotted as number of dead epithelial cells against iterations. As can be seen, they follow the same trends. Fig 2.6 (b) shows the mean and standard error of all ten simulation trials per iteration. The standard error was found to be 4.23 on average, with standard deviation of 2.97. Maximum standard error is 15.04. Therefore, the initial conditions do not significantly influence the course of the system.

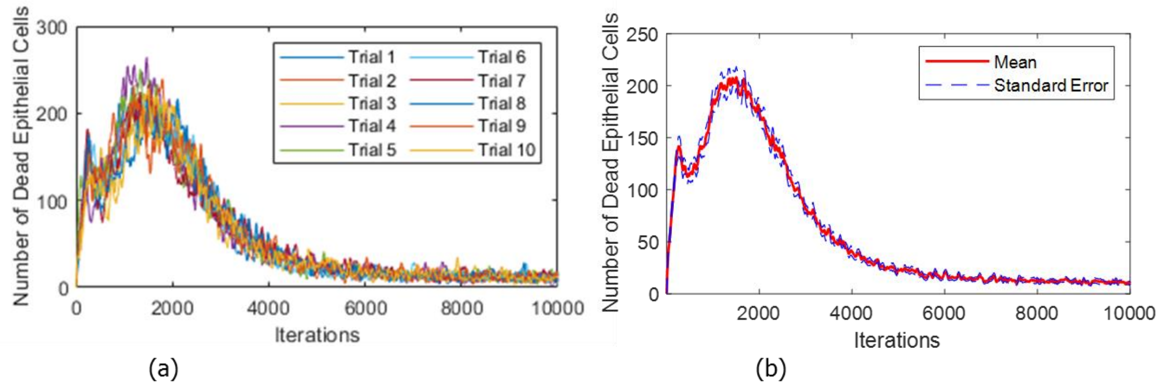

Figure 2.6: (a) plot of ten simulation results (number of dead epithelial cells) with the same parameters. (b) the mean of ten simulation trials taken for each iteration with standard errors.

2.6.3 Effect of Strain Magnitude on Cytokines Concentration

It is well established that airway and alveolar tissue respond to mechanical stimuli and there exists a correlation between increased strain magnitude and increased pro-inflammatory cytokines concentration [43][44]. Fig 2.7 shows TNF concentrations when the strain magnitude is increased. The TNF concentrations shown are averages of random samples (of 500 CA cells) from the whole CA grids, taken at different time steps.

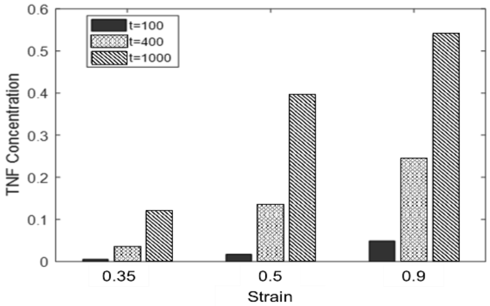

Figure 2.7: Evolution of TNF per strain, taken at three simulation points. The concentration is averaged for the whole CA grid, with 500 samples of CA cells.

It is well known that the average concentration of pro-inflammatory cytokines on the CA grid increases with the magnitude of strain. However, when the three data points were plotted and a low order interpolation was performed, it was found that the increases with respect to strain are linear in general.

2.6.4 Effect of Strain on Inflammation

Suppose we define an inflammation score by the number of dead epithelial cells during the course of the simulation. We present here the results of simulation with strains of 0.35, 0.5 and

0.9, which represent tissues under low, medium and high levels of strain. The strain experienced by tissue is subject to fluctuation during breathing. However, the time scale of breathing rhythm is much shorter than inflammation events (for instance, the breathing cycle has a period of four seconds, while inflammation may be apparent in days). Hence, the strain on the grid can be interpreted as the average strain during inflammation, and it was constant during the simulation. However, fluctuation of strains may also exist for other reasons (for example, when some part of the lung cannot accommodate sufficient airflow, the other parts will overstretch to compensate). Hence, we also present a case study where the CA grid experiences fluctuation of strain.

Fig. 2.8 shows ten samples of the evolution of dead epithelial cells after ten thousand time units, with the mean and standard error plotted. Notice the standard error lines have a noticeable gap in the lower strain case. As strain increased, the results showed less variance and thus thinner standard error gaps. One noticeable trend depicted in Fig. 2.7 shows that the number of dead epithelial cells increased quickly at the beginning, and stabilized later on. This is a consistent behavior irrespective of the level of strain on the CA grid. However, higher strain led to higher amplitude (higher number of dead epithelial cells).

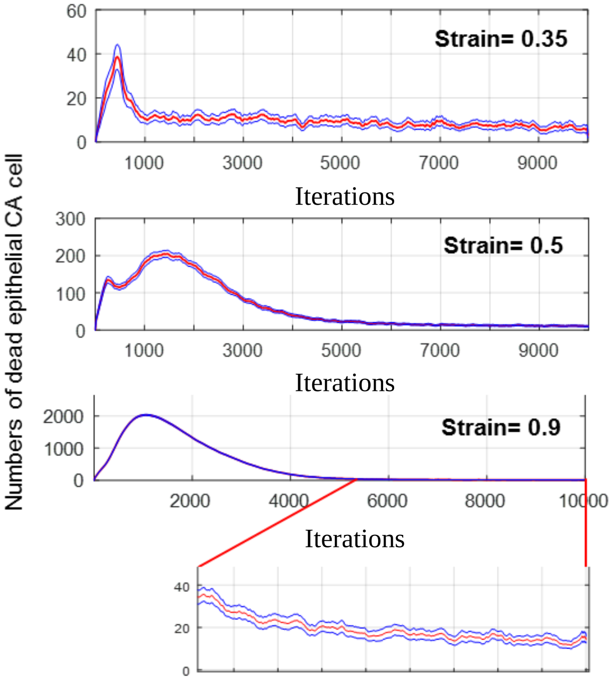

Figure 2.8: Inflammation over the course of time as represented by numbers of dead epithelial cells during the simulation. Thin-blue lines show standard error of 10 samples of simulations. Thick-red lines are the mean. Magnification of last plot (strain=0.9) is provided for clarity.

The CA also exhibited adaptive behavior and is apparent in the case of fluctuating strain. Fig. 2.9 shows the fluctuation of strain and the number of dead epithelial CA cells after one thousand iterations, again with the mean and standard error of ten samples of simulation for each case. It is apparent in the case of fluctuation with two peaks there is a suppression of inflammation during the second peak of strain (as can be seen from the approximately 45% lower number of dead epithelial CA cells during the second peak). This also appears in the other cases with more fluctuations: at some point during simulation there is apparent suppression of inflammation in response to later fluctuation. However, there remains some degree of inflammatory response (i.e., there are still some numbers of dead epithelial cells).

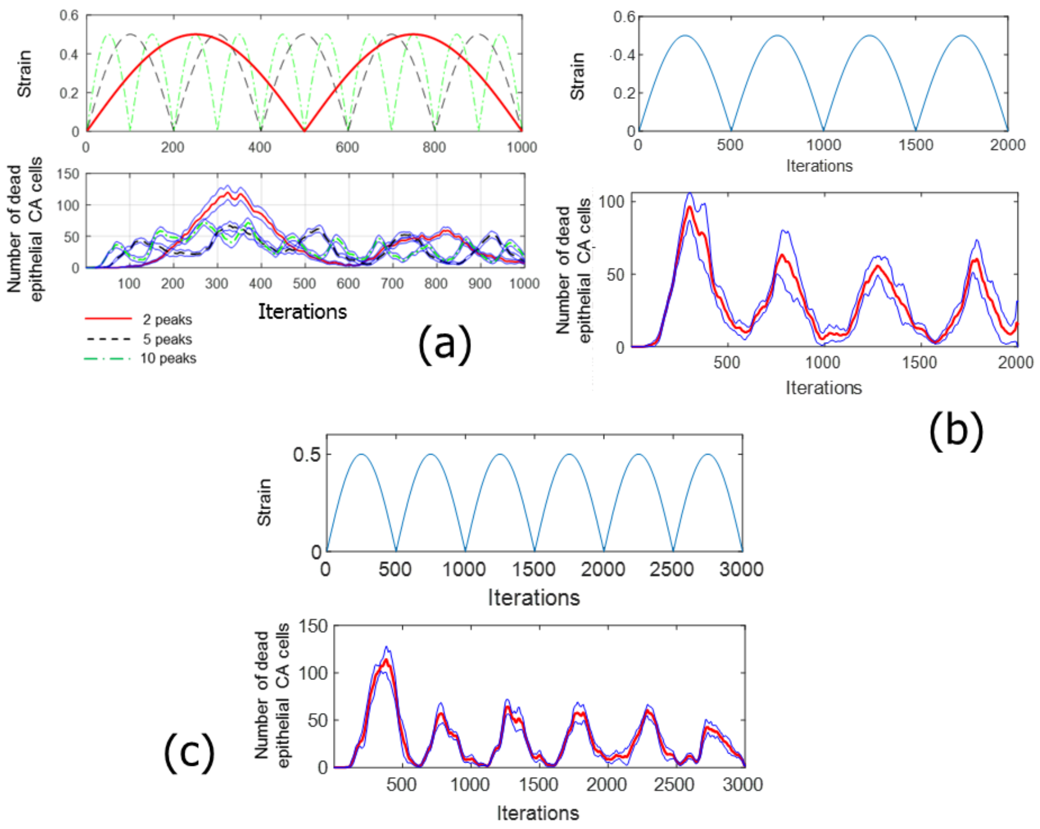

Figure 2.9: (a) Inflammation during strain fluctuation. Top: fluctuation of strains, with 2, 5 and 10 peaks. Bottom: motile response from the fluctuated strains. Thin-blue lines represent the standard error of 10 samples of simulation. Thick-red lines are the mean. (b) and (c) Extended simulations with more peaks of the fluctuating strains.

2.7 DISCUSSION

A CA model was developed based on the phenomenology of inflammation. The model takes into account the motility of motile cells, cytokines diffusion, and two damage events (apoptosis and fibrosis) and healing events (fibroblast and mitosis) on the epithelium. In this model, strain activates macrophages [31], which releases pro-inflammatory cytokines (TNF) [32]. TNF induces apoptosis [45] and signals fibroblasts [33] to release anti-inflammatory cytokine

(TGF) [33]. The TGF suppresses macrophages from releasing TNF and induces fibrosis on epithelium (causing damage). The model was tested with several cases, representing tissue experiencing low, medium and high strain under mechanical ventilation. The results were compared qualitatively with the phenomenology of inflammation. The model successfully emulated activator-inhibitor behavior [42] and strain-activated cytokines release [43][44]. Furthermore, the model successfully captured the qualitative behavior of inflammation in general (for an example case, refer to [46]).

Based on the results, there is a threshold of recovery from healing (as shown in Fig. 2.8). The damage on the tissue always went up until a certain point, and then was suppressed and later stabilized. The number of dead epithelial cells do not show a steady increase or decrease from that point onwards. This can be interpreted as the tissue and its constituents (as a system) reaching a new equilibrium. The damage exists, but the tissue has consistently recovered. The last case, where strain= 0.9, represents the extreme magnitude of strain, similar to the severely ventilated condition. One would have expected that higher strain would lead to the elimination of all epithelial cells. However, as can be seen in Fig. 2.8 for strain=0.9, only about 2% of epithelial cells (in a 100 by 100 grid of cells) undergo apoptosis, and the whole grid steadily recovers from the damage after time=2000. A portion of the epithelium is still damaged (by apoptosis) through the course of the simulation. However, it was suppressed and was “maintained” at minimum. This suggests the existence of an inflammation suppression threshold. It also suggests that this healing threshold is needed to maintain a minimum amount of apoptosis occurrence (minimum numbers of dead epithelial CA cells). Hence, some damage is needed to maintain optimum healing. Furthermore, the CA shows adaptive behavior as a response to fluctuating strain, as if early exposure of strain fluctuation helps the motile system to react during the latter fluctuation.

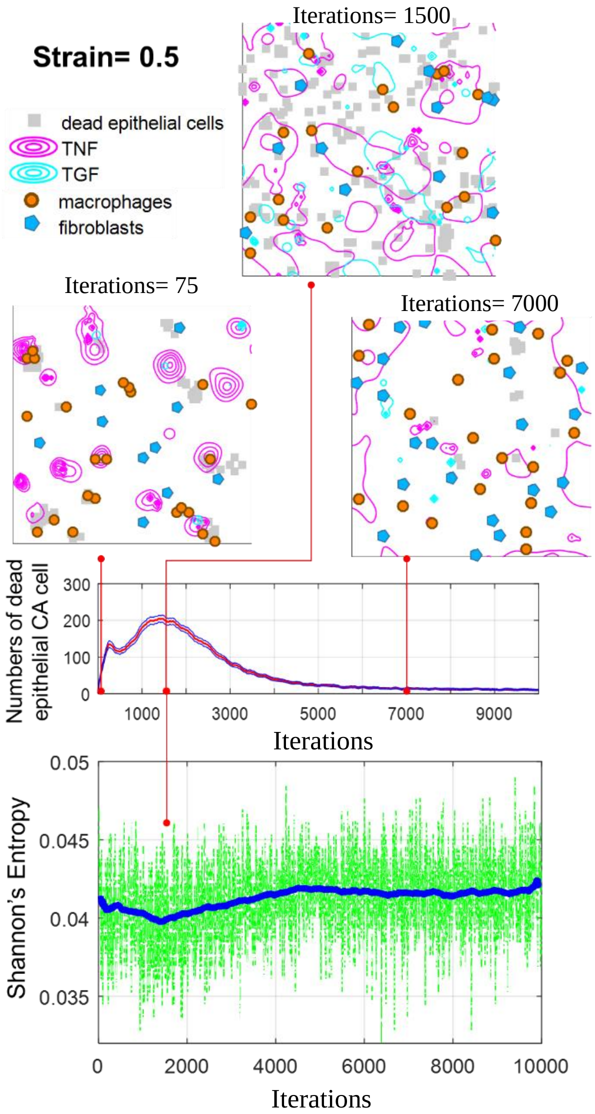

Figure 2.10: Top: Spatial distribution of motile cells. Suppression of inflammation (measured by numbers of dead epithelial CA cells) may have emerged from motile cells configuration and spatial distribution of cytokines. Bottom: Shannon's entropy of motile cells (macrophages and fibroblasts configuration during simulation. The background line (green) is original data, thick-blue line is smoothed data using moving average with span of 1000. The entropy of motile cells' configuration started to fall approximately at the peak of inflammatory response (around time=1500), and rose to stabilize when inflammatory response flattened.

The CA was built to model the innate immune system, and there is no explicit adaptive feature (such as memory in the adaptive immune system). Questions remain on the source of inflammatory response suppression and adaptive behavior shown. To explain this behavior, one can look at another aspect of CA simulation: the spatial distribution of CA cells (Fig. 2.10). At first, the motile CA cells seem to move randomly. However, by signaling (triggered by the presence of strain on the whole grid), the movements become less chaotic, more ordered. This is evident if one takes the spatial distribution of motile cells at each time step, and measures Shannon's entropy of the grid (Fig. 2.10). It is evident that the entropy dropped until it stabilized to a point during the course of the simulation. The movement of motile cells maximizing their entropy, and stabilizing after peak inflammation, suggests there are reconfiguration and convergence into a certain configuration.

Based on these results, we hypothesize that the adaptive behavior originates mainly from the spatial and temporal aspect of motile cells configuration. The motile cells, at some point during simulation, will converge into a certain configuration spatially. However, these motile cells died after some time, and the new motile cells arrived on the grid. But the old motile cells had left excess cytokines on the grid to be picked up by the new motile cells. This hastened the new cells to reconfigure on the grid. Thus, this behavior can be seen as an optimum propagation of signaling among motile cells spatially and temporally. This puts more importance on not only the spatial aspect of motile cells configuration but also the temporal aspect.

The model presented in this study successfully emulated the qualitative behavior of inflammation. In the future, the model can be extended for quantitative modeling by fitting the probability distribution with data from experiments. Furthermore, the model only considers two kind of cytokines and motile cells, and the outcome of subcellular process (such as chemotaxis and healing). The model can be extended by incorporating other tissue constituents and cytokines, as well as subcellular processes, and potentially provide more insights into inflammation dynamics.

2.8 CONCLUSION

A discrete informatics model based on the CA approach was developed to capture inflammation dynamics under different mechanical strain/stretch scenarios. The model takes into account certain aspects of inflammation, especially inflammatory mediators as expressed by different cytokines as well as existing experimental data. The simulation model investigated the effects of low, medium and high strain conditions on inflammation dynamics. Results suggest there is a threshold of innate healing capacity in tissue. The tissue as a system can suppress the inflammatory response; however, some degree of inflammatory response eventually remains. The visualization of the CA simulation grid revealed the spatial distribution of dead cells, fibroblasts, and macrophages. Visualization results also suggest that certain inflammation conditions would lead to a distinct pattern on epithelial cells. It will be interesting to pursue future research that will involve extending the current model to include other mechanisms as well as comparing patterns and results obtained from the simulation to imaging data or cellular experiments.

CHAPTER 3

COMPUTATIONAL SIMULATION OF CELL-TO-CELL COMMUNICATION DURING INFLAMMATION AND AGING

3.1 INTRODUCTION

The immune system relies heavily on signal transduction between cells [47-48]. Cells have two main methods of communication: by diffusive agents (e.g., cytokines) and active agents (e.g., cargo). An impairment in cell communication leads to all sorts of disorders and diseases [49-52]. Accordingly, it has been proposed that cells naturally form "social networks" [53]. In addition, spatial patterning and self-organisation of cells also emerges from diffusion-based communications [54]. Alteration of cell-cell communication is known to be associated with aging and consequently affects inflammatory response (termed inflammaging) [55], which consequently changes the collective dynamics. Furthermore, it can be reasoned that the course of inflammation might be determined by cell-cell interaction. Hence, analysis of cell-cell interactions may reveal insight into the fundamental aspects of inflammation as a process. Analysis of cell-cell communications within the scope of collective behaviours is important since new dynamics appear when cells move as part of a collective [56-57].

Due to its importance, several studies have analyzed cell-cell communication and its spatial and temporal aspects [58-60], including a microfluidic device with image-tracking developed to quantify spatio-temporal effects of macrophage and fibroblast communication [54]. A number of models have been devised to to analyze collective migration of cells through durotaxis [61-62] and chemotaxis [63-64] from the perspective of cells. These models enable cell migration description from mechanical and biochemical points of view. A statistical mechanics model of cell migrations was also devised to frame the analysis in terms of collective dynamics [65]. However, there is a lack of analysis from the point of view of information flow.

In a previous study [66-67], we investigated the migration of macrophages and fibroblasts during inflammatory response. Macrophages and fibroblasts were initially assumed as random-walking agents. However, once certain conditions are fulfilled and diffusive agents are released, their random-walk is biased toward a location in their neighbourhood with high concentration of cytokines (a simplification of chemotaxis). Inflammatory response normally leads to the recovery phase. However, due to aging conditions, the recovery (healing) phase may be delayed and lead to sustained injury (inflammaging).

In this study, we hypothesize that inflammaging as a process is dominated by macrophage collective dynamics where macrophages act as leader cells in the collective. To investigate this, we propose that cell-to-cell relationship in inflammaging can be modeled as a communication network, in this case, a bipartite network that maps the influence of macrophage into fibroblast (Fig 3.1(a)). To construct this communication network, we proposed a procedure to quantify information exchange between macrophages and fibroblasts. In this study, we applied this procedure to cell migrations data from an agent-based simulation tool for inflammatory response. Our procedure can be extended to experimental temporal data to map the relationship between agents and events in a complex process such as inflammation.

3.2 Materials and Method

3.2.1 Agent-Based Model of Inflammation

The agent-based model is a grid-based model similar to Cellular Automata. consists of multi-layered matrix representing different aspects of inflammation: the stimuli (strain), cells (epithelium, macrophages and fibroblasts), and cytokines. Each aspect has different rule to execute as described in the Method section. Some events are triggered by conditions fulfilled in other matrix. Fig 2.2 in Chapter 2 shows the PDFs (probability density function) of four

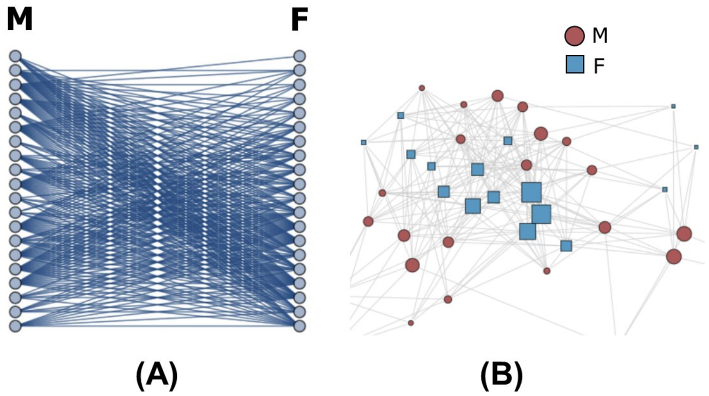

Figure 3.1: (a) Cell-to-cell communication is modeled as a map of influence from macrophage (M) to fibroblast (F) and vice versa. (b) A visualization of network centrality is shown here, where the size of nodes (red for macrophage and blue for fibroblast) corresponds to node's centrality. Higher node centrality means the node acts as a hub of information flow in the network since it can reach other nodes with minimum connection

main events in the in-silico model: likelihood of macrophage activation by strain (top), apoptosis by TNF level (top), likelihood of macrophage synthesizing TNF based on TGF level (middle), and likelihood of fibroblast synthesizing TGF based on TNF level (bottom). Table 3.1 presents the beta distribution parameters for these PDFs. Fig 3.2 shows all interactions between agents in the model. Arrow direction indicates the causal flow.

EPITHELIAL CELLS

Epithelial cells cycle their states between dead (by apoptosis) and alive. Apoptosis depends on the level of TNF [29]. The state transition rules are as follow,

1. All cells are initially alive.
2. A cell has probability to change its state to death in presence of TNF in its neighborhood. Higher TNF level significantly increases the chance of apoptosis. We model this likelihood by beta distribution function.

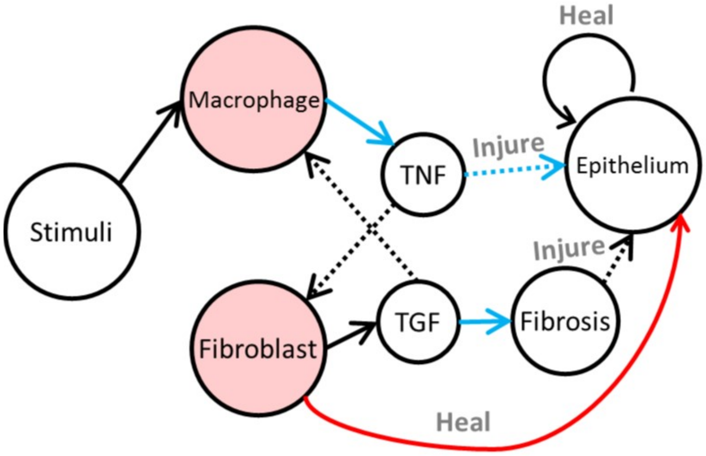

Figure 3.2: Interaction between component in Agent-based model of inflammation. Arrow indicate causal flow. Solid line indicates positive influence (activate, encourage). Dashed line indicates negative influence. Light red circle highlights the focus of this study. Blue arrows are events encouraged in the case of inflammaging. Red arrow indicates event impaired in inflammaging.

3. A cell changes its state to "alive" if at least a fibroblast present in its neighborhood. This healing process takes place for a specified amount of time, t_h (Point 11 in Table 3.1). After t_h time, a neighborhood of healed epithelial is randomly assigned a fibrosis site. Fibrosis site lasts for t_f time (Point 12 in Table 3.1).

4. A cell has probability to change its state to death if there is a fibrosis site in its neighborhood. The more fibrosis sites there are, the higher the probability. Hence, the probability is determined by N_f/N_{nei}, where N_f is number of fibrosis site in the neighborhood, and N_{nei} is the total number of neighboring cells. Neighborhood can be Moore's or Neumann's. This used to model risk of injury by fibrosis.

5. A cell has P_{mt} probability to change its state to "alive". This is used to model self-repair. The value was decided to account for its frequency relative to time step.

Therefore, there are two rules for apoptosis (Point 2 and 4) and two rules for healing (Point 3 and 5).

Motile Cells

Macrophages and fibroblasts are motile cells. Biological motile cells move by chemotaxis, and they signal each other through signaling protein (cytokines). Macrophages and fibroblasts are signaled by different cytokines [30]. In our model, macrophages are signaled by TNF (pro-inflammatory cytokine) and fibroblast by TGF (anti-inflammatory cytokine). Macrophages are activated by the presence of strains, and release TNF. Fibroblasts are activated by the presence of TNF, and release TGF. State transition rules are as follow,

1. Movements (random-walk): motile cells randomly move to an adjacent location the grid each time step. The random-walk is biased and the probability weights are determined from the associated cytokine's value in the cell's Neumann's neighborhood. A macrophage's random-walk bias is determined by values of TNF level obtained from TNF grid in the Neumann's neighborhood of said macrophage's site. Hence, when no cytokine presents, motile cells movement is non-biased random walk, with the only interaction is collision avoidance where each motile cell avoids occupying the same space as the others.

2. Activation: macrophages are activated by the presence of strains, and activated macrophages release pro-inflammatory cytokine (TNF). TNF release is probabilistic according to level of TGF. Its probability density function was inspired by report [32]. Fibroblasts are activated by the presence of pro-inflammatory cytokines, and release anti-inflammatory cytokine (TGF). TGF release is probabilistic according to level of TNF [33]. The likelihood of macrophage activation, TNF and TGF release are modeled by beta distribution functions.

3. Cytokine secretion: Each motile cell releases cytokine stochastically. The probability is defined by the level of associated cytokine's value located on the same grid coordinates as the motile cell. For example, the probability of a macrophage to release TNF is determined by value in the TGF grid located on the same grid coordinate as the macrophage.

Diffusing Cytokines

The cytokines in this model are assumed to be diffusing substance. There are two types of cytokines: the pro-inflammatory one (termed TNF) and anti-inflammtory cytokine (termed TGF). The rule is essentially a numerical solution of diffusion equation:

$$d\phi/dt = D.\nabla^2\phi - K.\phi$$

where ϕ is cytokine's concentration, D is diffusion constant that controls spread rate of cytokine, and K is dissolution constant that controls decaying rate of the cytokine. Typically, $D > K$.

Other Considerations

Physical variable is assumed static in this study, and hence each grid unit contains constant value throughout the simulation. For example, when simulation was run with strain of 0.2, the grid unit contained value of 0.2.

Inflammaging as Delayed Healing

In aging cases, the following parameters are modified:

1. Increase time delay of TNF synthesis by macrophage, t_M for aging condition 1 and 2. This is point 11 in Table 3.1.

2. A parameter of distribution function, β, increase the likelihood of TNF synthesis by stimuli. This is Point 9 entry of Table 3.1.

Table 3.1: Model Parameters (itr = iteration(s))

No	**Definition**	**Normal**	**Aging Case 1**	**Aging case 2**
1	Dimension of grid	100×100	100×100	100×100
2	Ratio of TNF to TGF diffusity, D_{TGF}/D_{TNF}	0.7	0.7	0.7
3	Ratio of TNF to TGF dissolution constant, K_{TGF}/K_{TNF}	0.01	0.01	0.01
4	Motile cell's velocity	1 grid/itr	1 grid/itr	1 grid/itr
5	Ratio of each immune cell population (macrophage or fibroblast) to total numbers of grid cells	0.002	0.002	0.002
6	Mitosis Probability, P_{mt}	1/5 itr	1/5 itr	1/5 itr
7	Macrophage activation by strain (beta distribution parameters)	$\alpha = 5$, $\beta = 1$	$\alpha = 5$, $\beta = 1$	$\alpha = 5$, $\beta = 1$
8	TGF syntheses by fibroblasts (beta distribution parameters)	$\alpha = 2$, $\beta = 1$	$\alpha = 2$, $\beta = 1$	$\alpha = 2$, $\beta = 1$
9	TNF syntheses by macrophages (beta distribution parameters)	$\alpha = 1$, $\beta = 3$	$\alpha = 1$, $\beta = 2$	$\alpha = 1$, $\beta = 1.5$
10	Epithelial cell apoptosis by TNF (beta distribution parameters)	$\alpha = 5$, $\beta = 1$	$\alpha = 3$, $\beta = 1$	$\alpha = 1.7$, $\beta = 1$
11	Macrophage's TNF synthesis delay, t_M	1 itr	7 itr	15 itr
12	Fibroblast healing time, t_h	5 itr	7 itr	15 itr
13	Fibrosis time, t_f	10 itr	15 itr	25 itr

3. A parameter of distribution function, β, to increase the likelihood of apoptosis. This is Point 10 entry of Table 3.1.

4. Decrease the time for fibroblast to heal an epithelial cell, t_h. This is Point 12 entry of Table 3.1.

5. Increase the time a fibrosis site lasts, t_f. This is Point 13 entry of Table 3.1.

3.2.2 Measure of Information Exchange

We used transfer entropy as a measure of information exchange between two temporal processes. Information entropy, H, can be defined as the amount of uncertainty contained within a random variable X,

$$H(X) = \sum_{x \in \mathcal{X}} p(x) \log p(x) \tag{3.1}$$

where $p(x)$ is the probability of X having the value of x in the set $\mathcal{X}$ of all possible values of X. As is typical in information theory, the logarithm used is base 2. Accordingly, the joint and conditional entropy can also be defined as follows,

$$H(X,Y) = -\sum_{x \in \mathcal{X}} p(x,y) \log p(x,y) \tag{3.2}$$

Transfer entropy is an extension of mutual information, which is a measure of common information shared between two random variables. Mutual information between random variable X and Y is expressed as,

$$I(X;Y) = H(X) + H(Y) - H(X,Y) \tag{3.3}$$

where $H(X)$ is information entropy of X, and $H(X,Y)$ is the joint information entropy of X and Y. Expanding the concept of mutual information, one can define conditional mutual information which is a measure of shared information between X and Y, given another variable Y',

$$I(X,Y|Y') = H(X|Y') + H(Y|Y') - H(Z,Y|Y') \tag{3.4}$$

In a temporal process, variable Y' can be Y at the previous time step. Hence, transfer entropy between X and Y is $I(X,Y|Y')$ and can be denoted as $T_{X \to Y}$.

3.2.3 INFORMATION EXCHANGE IN INFLAMMATORY RESPONSE

Inflammatory response is the result of signal transduction and coupling between many cells and events. We focus our study on macrophages and fibroblasts that are typically seen as agents with primarily conflicting roles. Macrophages typically are seen as a source of cytokine that exacerbate inflammation while fibroblasts are seen as agents of recovery.

To quantify the information exchange or communication between macrophage and fibroblast collective, it is necessary to consider the observable aspect of the temporal process. Migration properties such as directional persistence [68] have been used in the analysis of cell collective dynamics. In this study, the communication between macrophage and fibroblast was analyzed on the basis of their change of angle. The reasoning is that if there is an information transmission from a macrophage to a fibroblast, then it will alter the directionality of said fibroblast's migration. The direction of a cell can be represented as the angle between the current and previous path taken by a cell, i.e.,

$$\theta_{t,t-1} = \cos^{-1} \frac{m^t . m^{t-1}}{|m^t||m^{t-1}|} \tag{3.5}$$

where m^t is the vector of the path of a cell at time t (Fig. 3.3). We denote this angle as M_t and F_t for macrophage and fibroblast, subsequently. Transfer entropy, $T_{F \to M}$, between M_t and F_t can be defined as the mutual information between the two random processes conditional on a previous instance of M_t. It is expressed as,

$$\begin{aligned} T_{M \to F} &= I(F_{t-1}; M_t | M_{t-1}) \\ &= \sum_{M_t^i} \sum_{M_{t-1}^j} \sum_{F_{t-1}^k} p(M_t^i, M_{t-1}^j, F_{t-1}^k) \times \log \frac{p(M_t^i | M_{t-1}^j, F_{t-1}^k)}{p(M_t^i | M_{t-1}^j)} \end{aligned} \tag{3.6}$$

where $p(M_t | M_{t-1}, F_{t-1})$ is the probability of M_t given M_{t-1} and F_{t-1}. The probability of M_t, M_{t-1} and F_{t-1} are calculated by generating joint probability densities using binning specifications between 0.001 to 0.01.

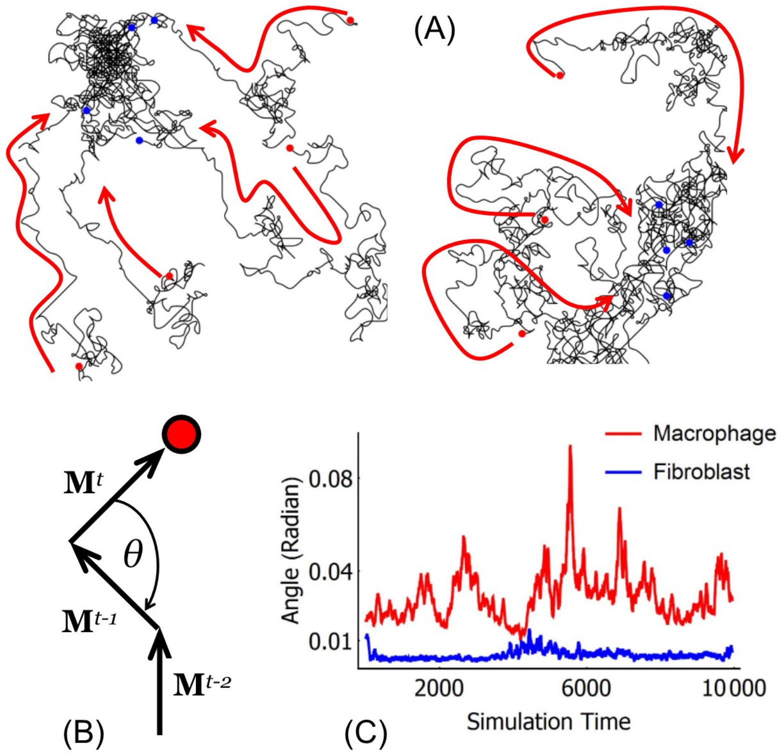

Figure 3.3: (a) Two samples of the migration track of macrophages and fibroblasts during inflammation after 500 time steps. They started as random walks, and as time progressed, the random walk became more biased and they converged in a common region. (b) Change of angle of a macrophage or fibroblast, as described in Sect 3.2.3. (c) a sample of change of angle of a macrophage and a fibroblast migrating over time.

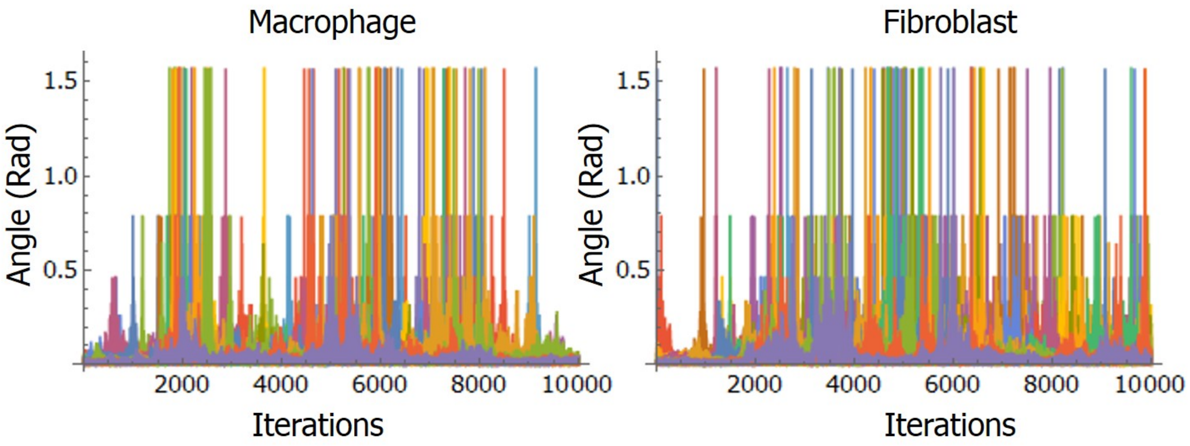

Figure 3.4: Migration data (angle of locomotion) of 20 macrophages and 20 fibroblasts used in this study

In this case, transfer entropy can be thought as the reduction in uncertainty of predicting the direction of a fibroblast at time step t given its previous direction (at $t-1$) and direction of a macrophage.

3.2.4 IMPLEMENTATION

The procedure of calculating transfer entropy, $T_{M \to F}$, is described below. Transfer entropy is based on the probability distribution of data. For example, Fig 3.4 shows angle of migration of 20 macrophages and 20 fibroblasts that were used in this study.

We denote $M_t^i = X$ and $M_{t-1}^j = Y$ as macrophage angle at time or iteration t and $F_t^k = Z$ as fibroblast angle at time or iteration t in the data. Joint probability distribution $p(M_t^i, M_{t-1}^j, F_{t-1}^k) = p(X, Y, Z)$ is calculated by binning the data in the form of $\{M_t^i, M_{t-1}^j, F_{t-1}^k\}$. The binning specifications of 0.001 to 0.01 was used based on Ref [69]. Transfer entropy expression can be simplified as [70]

$$
\begin{aligned}
T_{M\to F} &= \sum_{M_t^i}\sum_{M_{t-1}^j}\sum_{F_{t-1}^k} p(M_t^i, M_{t-1}^j, F_{t-1}^k) \times \log \frac{p(F_{t-1}^k) \times p(M_t^i, M_{t-1}^j, F_{t-1}^k)}{p(M_t^i, F_{t-1}^k) \times p(M_{t-1}^j, F_{t-1}^k)} \\
&= \sum_X \sum_Y \sum_Z p(X, Y, Z) \times \log \frac{p(Z) \times p(X, Y, Z)}{p(X, Z) \times p(Y, Z)}
\end{aligned}
\tag{3.7}
$$

The term $p(Z)$ and marginal probability, $p(X, Z)$ and $p(Y, Z)$, can be calculated from $p(X, Y, Z)$,

$$p(Z) = \sum_X \sum_Y p(X, Y, Z) \tag{3.8}$$

$$p(X, Z) = \sum_Y p(X, Y, Z) \tag{3.9}$$

$$p(Y, Z) = \sum_X p(X, Y, Z) \tag{3.10}$$

Using Eq. 3.8, Eq. 3.9 and Eq. 3.10, transfer entropy as in Eq. 3.7 can be calculated. Pseudocode of transfer entropy is provided in Appendix B.

3.2.5 VALIDATION AND SENSITIVITY ANALYSIS

Fig 3.5 shows plots of 10,000 points from three temporal random processes, named A, B and C. Process A and Process C are independent to each other, but B is created by from A by $B_t = (A_{t+1} + A_t)/1.85$. This yields data set B with comparable statistical properties (Table 3.2).

Therefore, we expect information transfer between A and B, with direction from A to B. When transfer entropy values between the three processes were calculated, the highest value was found to be transfer entropy from A to B ($A \to B$), while $B \to A$ is the second highest (Table 3.3). This results indicate that there is information transfer between A and B, with the direction is likely to be from A to B (highest transfer entropy value). The rest of transfer entropy values are the lowest between all calculated values, indicating low

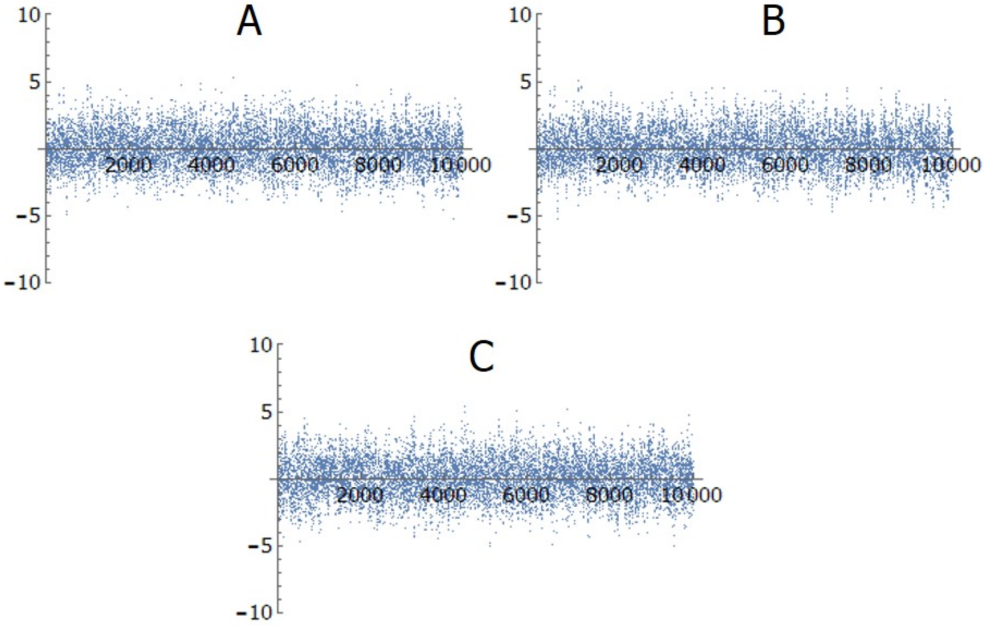

Figure 3.5: Data points of three Random Processes A, B and C to test transfer entropy approach.

Table 3.2: Statistical properties of A, B and C

Process	**Mean**	**Standard Deviation**	**Maximum**
A	0.012	1.4	5.29
B	0.013	1.4	5.05
C	0.019	1.41	5.35

information transfer. This example demonstrate that transfer entropy can be used to infer information transfer between temporal process and its direction.

Although A and C are two different processes, transfer entropy between them may still have values due to the nature of random processes. Thus, transfer entropy values are more useful with more data points. In this example, we tested transfer entropy with 10,000 data points and demonstrate that this amount of data points is enough to discern information

Table 3.3: Calculated Transfer Entropy Values of A, B and C

Direction	**Transfer Entropy**
$A \rightarrow B$	1.69
$B \rightarrow A$	0.34
$A \rightarrow C$	0.19
$C \rightarrow A$	0.19
$B \rightarrow C$	0.14
$C \rightarrow B$	0.19

transfer between A, B and C. The inflammation simulations in this study were carried out for 10,000 iterations.

3.2.6 Macrophage-Fibroblast (MF) Communication Network

Once the information exchange was calculated, the transfer entropy value can be used as a criterion to construct a communication network connecting a macrophage to a fibroblast, which is a bipartite graph, G_{MF} (Fig 3.1(a)). We refer this as MF network.

We iteratively removed edge in G_{MF} according to a pair's $T_{M \rightarrow F}$. If a pair of macrophage and fibroblast yields $T_{M \rightarrow F}$ below a certain threshold T_C, then an edge between them is not included in G_{MF}. This rule can be expressed as,

$$f(M_i, F_i) = \begin{cases} \{M_i, F_i\} \in G_{MF}, & T_{M_i \rightarrow F_i} > T_C \\ \{M_i, F_i\} \notin G_{MF}, & T_{M_i \rightarrow F_i} \leq T_C \end{cases}$$

where $\{M_i, F_i\}$ denotes an edge between two nodes, M_i and F_i. We derived T_C from the estimated distribution of $T_{M \rightarrow F}$. Since $T_{M \rightarrow F}$ is calculated for every pair of macrophage and fibroblast, a $T_{M \rightarrow F}$ distribution can be estimated. Based on $T_{M \rightarrow F}$ distribution, we took the most likely $T_{M \rightarrow F}$ values for edge generation criterion. We define a range of values with the mode of distribution as a point of reference. In this case, we used the first and third quartiles of $T_{M \to F}$ distribution as the criterion of edge inclusion and to account for asymmetry of the distribution.

To identify the dominant actor in the MF network, we estimate the Betweenness Centrality, C_B. Nodes with high centrality can find shorter paths to other nodes to cover the whole network. Thus, in terms of information flow, nodes with higher centrality can easily signal and influence other nodes, similar to the role of a leader. Betweenness centrality of a node, $C(v)$, is given by [22],

$$C(v) = \sum_{i \neq v \neq j} \frac{\sigma_{ij}(v)}{\sigma_{ij}} \tag{3.11}$$

where σ_{st} is the total number of shortest paths from node s to node t and $\sigma_{st}(v)$ is the number of those paths that pass through v. Nodes with high centrality can find shorter paths to other nodes to cover the whole network. Thus, in terms of information flow, nodes with higher centrality can easily signal and influence other nodes.

3.2.7 Migration Data of Macrophage and Fibroblast

To obtain the temporal change of angle of macrophage and fibroblast, we employed agent-based simulation as presented in our previous study [66-67]. The agent-based simulation is able to capture the typical time course of inflammatory response, where a sudden rise in inflammation score is followed by a steady decline until inflammation scores are negligible.

To simulate aging, we induced delayed healing [71-72] in the simulation. Aging is characterized by an increased level of pro-inflammatory cytokine [73], impairment of wound repair and tissue regeneration [72], and prolonged fibrosis [74-75]. Thus, we set the model parameters reflecting these conditions: regulation of pro-inflammatory cytokine synthesis (encouraged), apoptosis (encouraged), regeneration rate (impaired) and period of fibrosis (prolonged). Fig 3.6 shows simulation results of inflammaging. It can be seen that for inflammaging cases, the inflammation scores did not decline immediately and were not followed by full recovery (i.e., inflammation score were still apparent).

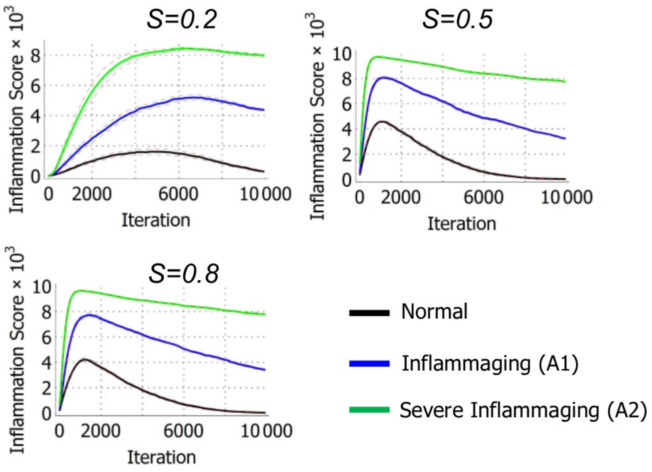

Figure 3.6: Time course of inflammation under different levels of stimuli, S. Each time course is an average of 10 simulations. For Normal cases, the time course always ends with complete recovery as inflammation score becomes negligible toward the end of the simulation. For inflammaging cases, some degree of sustained injury will be present. Each inflammation time course is associated with certain macrophage-fibroblast information exchange.

To explain the inflammaging time course in terms of cell-to-cell communication, we extracted the temporal change of angle of macrophage and fibroblast. A sample of motile cell migration is shown in Fig 3.3(a). Fig. 3.3(a) shows the path of some motile cells after 500 iterations. Motile cells initially exhibit random walks, but as can be seen in Fig 3.3(a), the movements of motile cells were converging into particular regions after a certain time. This convergence corresponds to the time the cytokines took to spread over the grid by diffusion. Fig 3.3(b) illustrates the scheme for calculation of change of angle, as explained by Eq. 3.5 in Sect 3.2.3. Fig 3.3(c) shows a sample of change of angle of randomly chosen macrophage and fibroblast plotted over time.

For the purpose of this study, we carried out agent-based simulations and extracted the tracks of macrophages and fibroblasts at each time step. The simulations involved 20 macrophages and 20 fibroblasts. The simulations were carried out under three level of stimuli, S= 0.2, 0.4 and 0.8, and three aging progressions, termed Normal (N), Inflammaging ($A1$)

and Severe Inflammaging ($A2$). In addition, simulations with no stimuli were also carried out for comparison.

3.3 RESULTS

Inflammation time course for all aging cases and stimuli level are shown in Fig 3.6. The zero stimuli $S = 0$ cases do not provoke any response, because no signaling cytokine was released and diffused. It can be seen in Fig 3.6 that the inflammation score (i.e., level of injury) for inflammaging cases are worse than Normal cases, and the scores for inflammaging A1 are worse than A2. Thus, for the purpose of discussion, we named the order of aging progression as $N > A1 > A2$.

We repeated simulations of each stimuli level and aging progression for ten times. Fig 3.7 shows the estimated distribution of $T_{M \to F}$ for each inflammation time course. As can be seen, when no stimuli are present, the $T_{M \to F}$ is close to zero (red lines). This is expected since in this case, there is signaling involved in the macrophages and fibroblasts migrations. Inflammaging ($A1$ and $A2$) shifts the $T_{M \to F}$ toward zero (Fig 3.7, middle and right) such that they overlap with no-stimuli $T_{M \to F}$ distribution. Thus, migration dynamics of cells becomes progressively dominated by random walk as aging progresses, and implies weak information exchange between macrophage and fibroblast under inflammaging.

We constructed MF network for each case of inflammation. Fig 3.8(b) shows the estimated betweenness centrality distribution of macrophage and fibroblast for all ten simulation trials. The most prominent feature in Fig 3.8(b) is the opposite preference between macrophage and fibroblast nodes due to inflammaging. As inflammaging severity advances ($A1$ (green) to $A2$(red)), the likelihood of high centrality nodes on macrophage side raised, while fibroblast nodes declined (the shifts are illustrated by arrows in Fig 3.8(b)). This conflicting relationship applies to all stimuli level. In addition, the $S = 0$ cases have less preference of centrality (Fig 3.8(b), dashed line).

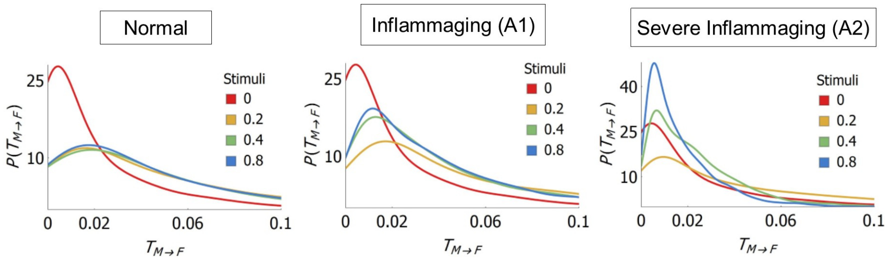

Figure 3.7: Distribution of $T_{M\to F}$ for each inflammation time course under Normal condition (Left), Inflammaging (Middle) and Severe Inflammaging (Right). For simulation with no stimuli (red lines), the $T_{M\to F}$ is likely to be near zero. As inflammaging progresses from $A1$ to $A2$, the $T_{M\to F}$ shifts toward zero as well, indicating weak information exchange between macrophage and fibroblast.

The shifts in centrality distribution by stimuli level are not apparent as seen in Fig 3.8(b). Hence, we calculated the ratio of maximum macrophage and fibroblast nodes centrality (denoted as F and M, respectively) and averaging over all ten simulation trials for each case. Fig 3.9 shows the ratio, F/M. As can be seen in Fig 3.9, F/M fell below 1.00 with aging conditions, indicating the shift of centrality from fibroblast part to macrophage one. In terms of stimuli level, although the shift in distribution is slight, the preference of centrality can be observed in terms of F/M. As seen in Fig 3.9, the networks for aging cases lead to $F/M < 1.00$ in general, indicating centrality is more likely on macrophage part. In Normal cases, F/M is always bigger than 1.00, indicating centrality is more likely on fibroblast part. Hence, we have a divergent trend in terms of stimuli level.

3.4 Discussion

In Fig 3.6, we found that inflammation time course in Normal cases eventually ends with full recovery, while Aging 1 and Aging 2 leads to sustained injury of different intensity. Based on Fig 3.6 and Fig 3.8(b), it is possible to associate node centrality in MF network with the course of inflammation.

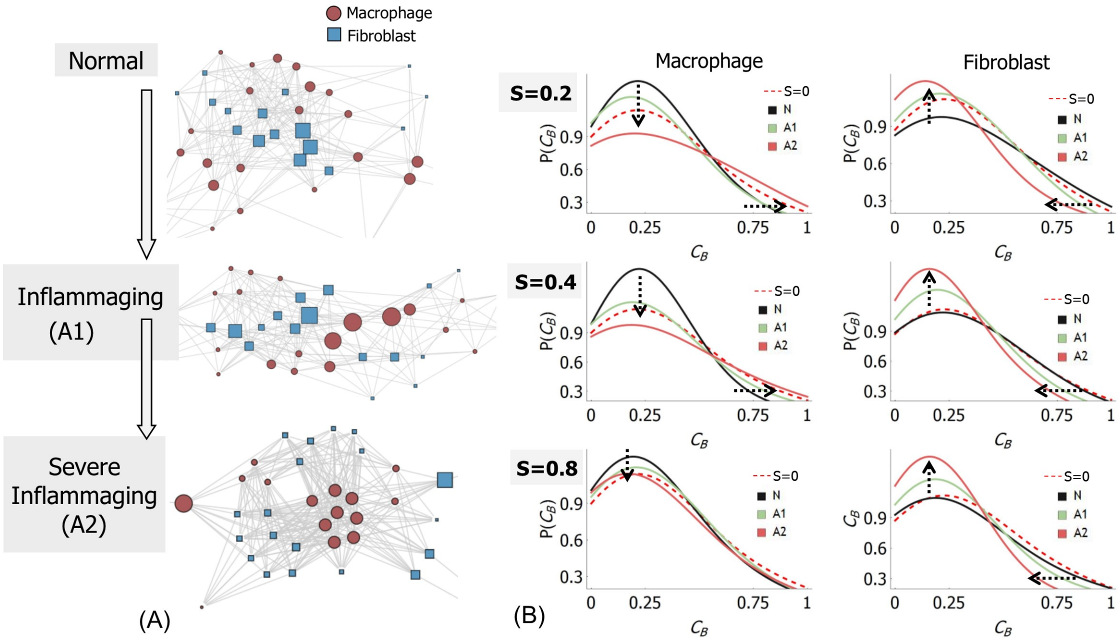

Figure 3.8: (a) A sample of macrophage-fibroblast communication networks representing inflammation (N) and inflammaging ($A1$ and $A2$). Red nodes denote macrophages while blue nodes signify fibroblasts. Size of the nodes indicates the centrality of each node. It can be observed that for inflammaging, macrophage node's centrality, in general, are higher than fibroblast nodes, indicating macrophages dominate the collective system in inflammaging. (b) Distribution of centrality, C_B, for different inflammation time course and stimuli. For all stimuli levels, S, inflammaging causes the shift of centrality of MF network as indicated by arrow: higher centrality on macrophage nodes (left) and lower centrality on fibroblast nodes (right).

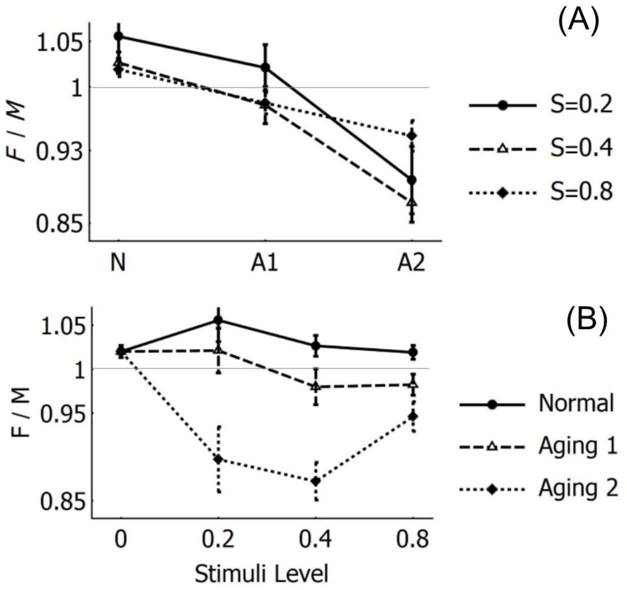

Figure 3.9: (a) The ratio of fibroblast and macrophage centrality, F/M of the MF networks for each inflammation time course (N denotes Normal inflammation, $A1$ denotes Inflammaging and $A2$ denotes Severe Inflammaging). F/M declines as the severity of inflammaging advances, which indicate the shift of centrality from fibroblast, F, to macrophage, M. The trend holds for all stimuli level. (b) The same data arranged according to stimuli. Stimuli levels also shift centrality to a degree but not as significant as the severity of inflammaging.

All inflammation followed by full recovery appears to have MF networks with lower centrality in macrophage nodes, shifting the centrality toward fibroblast nodes. A sample of these networks is visualized in Fig 3.8(a), marked as Normal. Inflammation that leads to sustained injury (Inflammaging) tend to have MF networks with opposite preference: higher centrality in macrophage nodes. Samples for the latter case are visualized in Fig 3.8(a), marked as $A1$ and $A2$, respectively. Therefore, the fate of inflammation (i.e., full recovery, or sustained injury) can be associated with the topology of the MF network.

The MF networks presented here may have encoded the primary role of the agents in the system, or the degree to which agents drive the system. Fibroblast is assigned as an agent that administers healing and suppresses inflammatory cytokine. Hence, the preference of centrality to the fibroblast nodes in full-recovery cases might be indicative of its role. It might also indicate that fibroblasts were the primary driver of the system for those cases. Similarly, the macrophage is assigned as an agent that exacerbates inflammatory response and primary motivator of injury. Preference of high centrality nodes in macrophage side may be indicative of its role or influence to the system.

Another interpretation of the results is that macrophage-fibroblast MF network may govern the course of inflammation (i.e., full or partial recovery). Consequently, the course of inflammation may be modified by altering macrophage-fibroblast MF networks. Information exchange estimated in this study is not solely driven by cytokines secretion and diffusion, but also environmental factors such as, such as motile cell velocity and local density. A motile cell avoids collision with each other and a crowded area can deter the movement of motile cells. In real circumstance, biological fibers are also known to deter motile cells migration, impairing immune response [76]. Thus, information exchange between macrophage and fibroblast can be altered by modifying mechanical and environmental factors. Some authors have reported methods to alter cell-cell interactions through mechanical means [12][15][77-78].

3.5 Limitation

The migration data in this study were obtained from agent-based model. The motion of agents in the model were limited to eight cardinal directions and hence the migration data had limited and discrete angles.

3.6 Conclusion

The time course of inflammation relies on communication between cells. In this study, we presented a method to model macrophage-to-fibroblast communication in inflammaging, which we call as MF network. We demonstrate that the MF network characterised the time course of inflammation. Normal inflammation yields MF network that indicate fibroblasts are the collective leader of the system, while inflammaging yields MF network that indicates macrophages dominate the collective dynamics. This is expected since macrophages are primary agents that exacerbate inflammatory response. Mapping the relationships between coupled agents or events are important to determine which process to amplify or suppress.

CHAPTER 4

NETWORK MODELING AND ANALYSIS OF BRONCHOCONSTRICTION

The pulmonary system is a natural network of airway tubes, a fluidic transport network that forms a tree structure. Environmental and genetic conditions may cause obstruction of a number of airways in the system (termed bronchoconstriction). This may happen through an inflammatory response that leads to thickening of the airway lumen, leading to airway narrowing. When bronchoconstriction occurs, the lung ventilation (i.e., the volume of air reaching a region of the lung) becomes irregular or defective [79][80]. In another study, a framework for growth on a networked system has been proposed [23]. Under this framework, local growth is important to a networked system to achieve optimized, steady state connections. In this study, we proposed that bronchial constriction may arise from the same process. Since the airway tree can be naturally represented by a mathematical graph, we investigated the relationship between this process and graph (network) properties. We proposed a network-centric approach of the respiratory airways that can be used for morphological study of the lung in relation to disease. An overview of the approach of bronchial constriction quantification using adaptive network model and their network measures is shown in Fig 4.1.

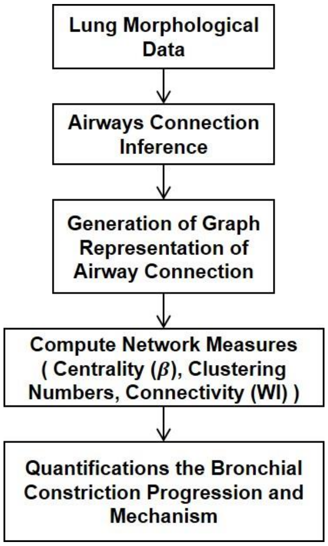

Figure 4.1: An overview of the approach for bronchial constriction quantification

4.1 METHOD

In this section, the computational approach for modeling airflow in the airway tree is presented. The lung airway system was treated as a tree graph, where airway conductance acts as edge weight in the tree graph, and Kirchoff's law governs the flow. The mechanism of airway network adaptive behavior was inspired by the mechanics of canalization in plant venation. Next, we employed an informatics approach to analyze the final connectivity of airways by estimating graph measures.

4.2 MODEL OF AIRFLOW

Physiologically, the bronchial tree consists of bifurcating airways that start with the trachea. Each airway tract bifurcates 23 times. We termed each bifurcated airway as a generation number and the trachea as generation 0 (G0). This is illustrated in Fig 4.2(a).

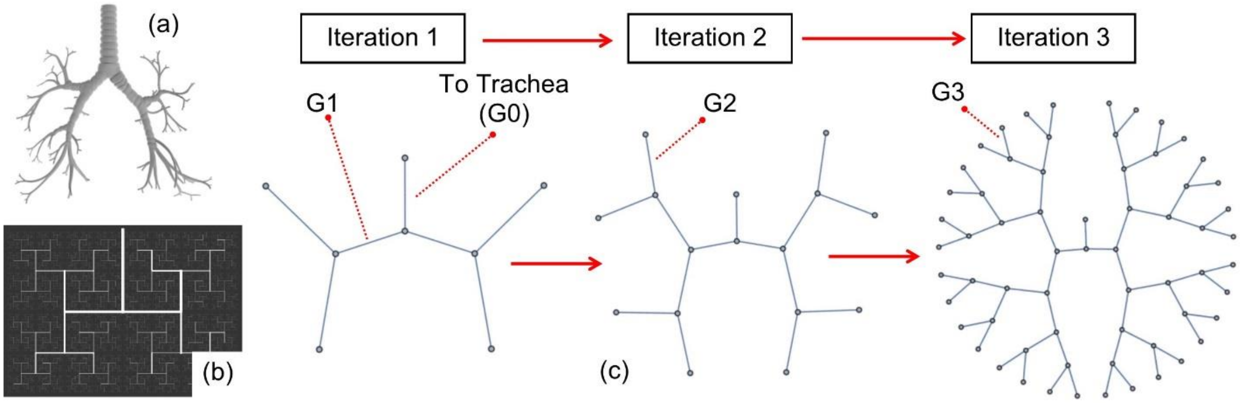

Figure 4.2: (a) a three dimensional model of a pulmonary tree. (b) It can also be visualized as a Mandelbrot-like fractal. (c) The pulmonary tree is modeled as a tree network. The tree network generation is illustrated here, started from generation zero (trachea). The iteration is continued until generation 12.

Each airway in the tree network resists the airflow. The resistance, R, is given by [81], [82],

$$R = \frac{8\mu l}{\pi r^4}\left(Re\frac{D}{l}\right)^{1/2} \tag{4.1}$$

where μ is air viscosity, Re is Reynold's number, l and r are length and radius of an airway unit, respectively, and $D = 2r$. To simplify the problem, we reduced the scale of the bronchial tree to 12 generations. The resistance can be calculated for airways of all generations based on morphological characteristics of airways (i.e., radius and length). These parameters are given in [83]. By assuming Pousiville's flow, the flow through the network is,

$$\mathbf{Lp} = -\mathbf{S} \tag{4.2}$$

where $\mathbf{L}$ is the Laplacian matrix of a graph domain, $\mathbf{p}$ is a vector of node potential, and $\boldsymbol{S}$ is the node source. Although the simplifying assumption may not accurately describe the flow in the upper part of the airways (Generation 0-5), some models were developed through this assumption to characterize airflow in lung [82][79].

We assume the node representing the trachea (Fig 4.2(b)) as the source of air flow, and thus modeled it as a current source. The alveoli pressure is designated as the ground nodes and hence the rest of the graph periphery (end nodes of the graphs in Fig 4.2(c)) is assumed as zero potential. The node potentials, $\mathbf{p}$, across the graph domain are then solved through Eq. (4.1). Once node potentials are solved, the edge flow, $\mathbf{I_e}$ is,

$$\mathbf{I_e} = \mathbf{K} \cdot \mathbf{P_e} \tag{4.3}$$

where $K = R^{-1}$ is conductance matrix, $\mathbf{p_e} = \mathbf{A}.\mathbf{p}$ is edge potential, and $\mathbf{A}$ is the incidence matrix of the graph. $\mathbf{L}$ is related to $\mathbf{A}$ by $\mathbf{L} = \mathbf{A^t}.\mathbf{K}.\mathbf{A}$.

4.3 MODEL FOR NETWORK ADAPTATION

In this study, a known phenomenon in asthma is used as the basis of model formulation. During ventilation defect, the collective lung airways adapt their morphological characteristics in response to decreased airflow in the whole lung (ventilation) [84]. As a consequence, the airflow and ventilation distributions are affected.

This self-organization of the airways is arguably similar to another phenomenon of self-organization in canalization in plant venation [23]. In response to flow, plant venation adapts the lumen to allow more flux in the same path. The change in lumen radius is thought to be mainly driven by shear stress on venation wall. A general model for this dynamics was proposed in [23] as,

$$\frac{dK_i}{dt} = a(I_i)^{2\gamma} - bK_i + c \tag{4.4}$$

where K_i is conductance of each edge, I_i is flow at the edge, and a, b, c, and γ are constants. Eq. 4.4 can be non-dimensionalized by using the scaling factor definitions and the following dimensionless expressions,

$$\bar{I} = I/\hat{I}\,,\;\; \bar{p} = p/\hat{p},\;\; \bar{t} = (1/\hat{b})\hat{t},\;\; \bar{K} = \frac{b'}{a}\left(\frac{\hat{I}}{\hat{p}}\right)^{2\gamma}\;\hat{K} \tag{4.5}$$

The dimensionless form is,

$$\frac{d\hat{K}_i}{dt} = \hat{I}_i^{2\gamma} - \hat{K}_i + \kappa\, e^{(-\hat{t}/(1+\rho))} \tag{4.6}$$

where $b' = b + r\delta\gamma$, $\kappa = \left(\frac{c}{a}\right)\left(\frac{\hat{I}}{\hat{p}}\right)^{2\gamma}$ and $\rho = b/(r\delta\gamma)$. The last two dimensionless parameters control the dynamics of Eq. 4.6 [23]. In a tessellated network, this system leads to two phase: highly connected network at low κ and ρ, and hierarchical networks at high κ and ρ.

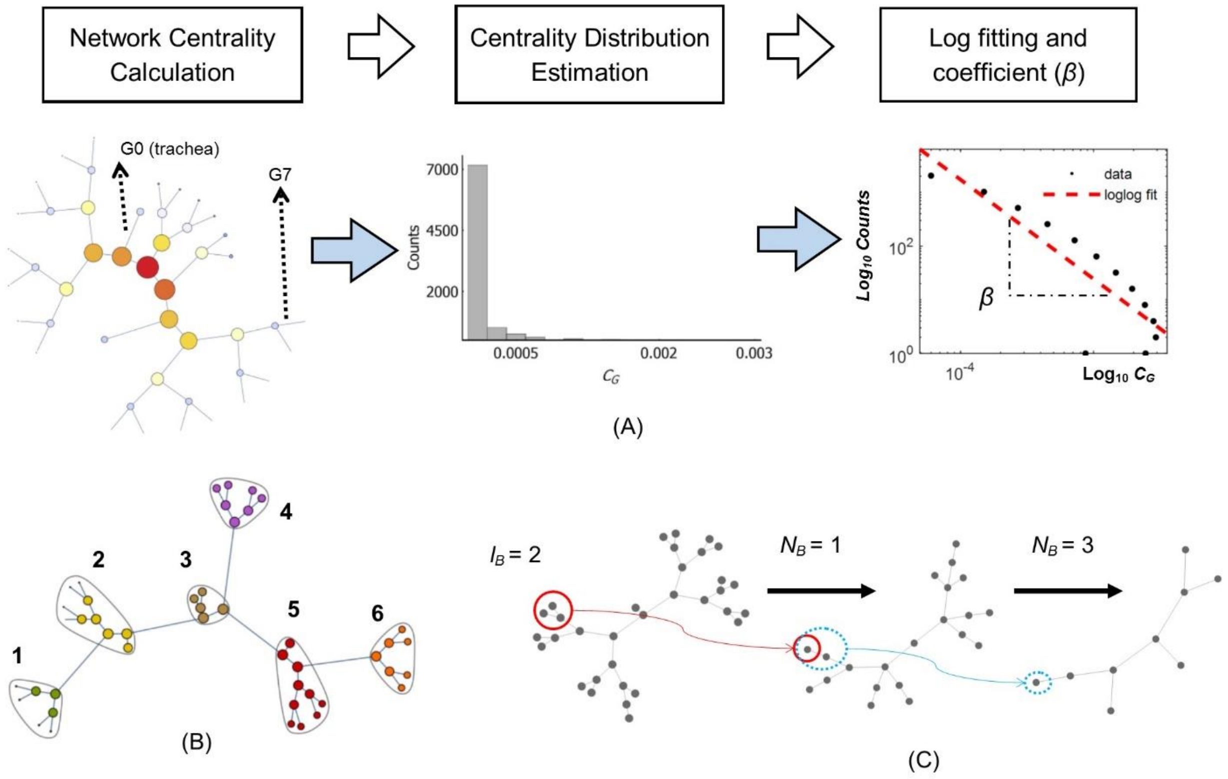

Figure 4.3: (a) Procedure to obtain β as a characterization of network centrality. A visualization of eigenvector centrality in a fraction of airway tree network is also shown. Higher node size indicates higher centrality. (b) A sample visualization of network cluster based on community detection algorithm for the same airway network in (a). In this example, the airway network has six clusters. (c) A sample of network renormalization/coarse-graining iteration of an airway tree network by CBB algorithm used in this study. The algorithm starts with a randomly selected node (red circle) and its neighbor separated at least $l_B - 1$ degree. This node and its neighbors is reduced into one node in the first step ($N_B = 1$). The process applies to all nodes and is repeated until only a node left ($N_B = 8$ in this example)

4.4 MEASURE OF AIRWAY NETWORK COMPLEXITY

A fundamental measure of a network is its node degree. Node degree is the number of connection a node has to other nodes. By the nature of the airway network, each node will mostly have a degree of three, since each airway is connected to three other airways (Fig 4.2(c)). Bronchial constriction alters the airway connectivity since some airways will be constricted and disconnected to the rest of the network. We consider several network measures to characterize the normal and altered airway network.

4.4.1 EIGENVECTOR CENTRALITY

Centrality is a measure of the importance of a node to the whole network. In eigenvector centrality, a node that is connected to many other high centrality node will score high in centrality. Eigenvector centrality c_i of a node i is described by [85],

$$\mathbf{A}\,\mathbf{c} = \boldsymbol{\lambda}\,\mathbf{c} \tag{4.7}$$

where **A** is the adjacency matrix of the graph describing the network, and λ is the largest eigenvalue of **A**. Fig 4.3(a) visualizes centrality of a sample airway tree network that has undergone bronchial constriction and thus is asymmetric. For the full (unaltered) airway tree network (as in Fig 4.2(c), the node centrality distribution is shown in Fig 4.3(b). We characterized this distribution by fitting it into log-log relationship (Fig 4.3(a): middle and right) according to,

$$f(x) = 10^{\alpha} x^{\beta} \tag{4.8}$$

We characterized the centrality by the power β. As a reference, the original (unaltered) airway network has $\beta{\sim}1.85$ (Fig 4.3(a): middle and right).

4.4.2 WIENER INDEX

We also considered the Wiener index as network connectivity measure. It is described by [22],

$$W = \frac{1}{2}\sum_{v_i}\sum_{v_j}\mathbf{D}(v_i, v_j) \tag{4.9}$$

$$\mathbf{D}(v_i, v_j) = \min_{\prod i,j}\sum_{e_{ij}\in\prod i,j} w(e_{ij}) \tag{4.10}$$

where v_i is node i, $\mathbf{D}(v_i, v_j)$ is graph distance matrix, $w(e_{ij})$ is the weight of the edge e_{ij}, and $\prod i,j$ is a set of edges connecting v_i with v_j. The Wiener index is the sum of the shortest path lengths between any pairs of nodes in the network. A small Wiener index indicates a more well-connected network compared to other networks with a similar number of nodes having a large Wiener index.

4.4.3 NETWORK CLUSTER

To measure clustering in the network, we used the concept of community structure in a network. A community can be thought of as a cluster of nodes with more in-group connectivity than out-group connectivity. Community detection is computationally difficult and requires algorithms [86]. A well-known algorithm is based on a measure called modularity [86]:

$$Q = \frac{1}{w_t}\sum_{ij}\left(A_{ij} - \frac{d_i d_j}{w_t}\right)\delta(i,j) \tag{4.11}$$

where w_t is the sum of all edge weight in the network, d_i and d_j is the degree of node i and j, respectively, δ is delta function with respect to iterator i and j. The modularity Q can be positive or negative-valued, with higher positive value indicates a stronger assignment of two nodes i and j in a community. In this way, the task of community detection becomes a problem of maximizing modularity Q for a given division of network nodes. Fig 4.3(b) shows an example of network clustering of an airway tree into six clusters.

4.4.4 NETWORK RENORMALIZATION

Network renormalization can be thought of as an iterative coarse-graining of a network, similar to measurement of fractal dimensions of a data set. However, when reversed, the process is analogous to a growth model, and it has been described as a model for fractal network growth mechanism [87]. A mathematical model that described this process is,

$$N(t) = n\,N(t-1) \tag{4.12}$$

where $n > 1$ is a rate constant. This equation is analogous to a typical discrete time population growth model [88]. However, for a given network, renormalization can be described by an algorithm similar to finding the fractal dimension of a graph describing a network. It can be used to identify the structure underlying a network (e.g., whether a network is fractal and modular or not) and its robustness [87].

In this study, we hypothesized that bronchial constriction progression may share characteristics with network renormalization. Hence, we employed a renormalization algorithm on altered (constricted) airway network for comparison with the full, unaltered airway tree. Among the numbers of algorithms proposed, the Compact Box Burning (CBB) algorithm is the fastest in terms of performance and implementation without losing accuracy [89]. For a given network, G, with nodes N, the CBB algorithm is calculated following these steps,

- Start with a set of all uncovered nodes, U
- Select a random node i from the set U and remove it from U

- Remove all nodes j whose distance l_B from i is $l_B \leq L_i$, where L_i is a threshold of distance
- Repeat the second and third step until U is empty

Through this algorithm, a network of N nodes is iteratively coarse-grained into a graph with fewer nodes by grouping neighboring nodes separated by $l_B - 1$ into N_B number of boxes. This process is illustrated in Fig 4.3(c). In this study, L_i is determined to be 2.

4.5 IMPLEMENTATION

To solve the flow in all nodes, Eq. 4.2. Runge-Kutta method was used to solve Eq. 4.6. A simulation was run until convergence was achieved. Convergence criteria are met when the solutions from the current and previous time steps are close enough (i.e., $\bar{p} + \sigma_p < 10^{-10}$, where $\bar{p}$ and σ_p are the mean and standard deviation of $\mathbf{p}^t - \mathbf{p}^{t-1}$, respectively, and $\mathbf{p}$ is the solution of Eq. 4.2). To induce bifurcation in the system, the conductance K_i was varied by randomizing the diameter and radius from the baseline values (see Eq. 4.1) with a variance σ of 0.01.

MATLAB 2018 was used to solve Eq. 4.2 and 4.6, while network analysis was carried out using Mathematica 10 using its built-in network analysis package. Simulation experiments were carried out to determine the value of κ and ρ that yields tree network that corresponds to patchy, defective ventilation distribution. The values are ρ=0.625 and κ ranging from 0.16 to 3.2.

4.6 RESULTS

4.6.1 VALIDATION

We compared the simulation results with previous results on pattern formation during bronchial constriction. The main feature of bronchial constriction is that the distribution of ventilation is polarized and ventilation defects are clustered [79][84]. We defined indication of relative ventilation here as the ratio of local edge flow, $\mathbf{I_e}$, of the constricted network to the original one. This ratio is termed Ir in Fig 4.4. In Fig 4.4 (b) and (c), the polarized distribution of Ir is clearly evident as observed in bronchial constriction [79].

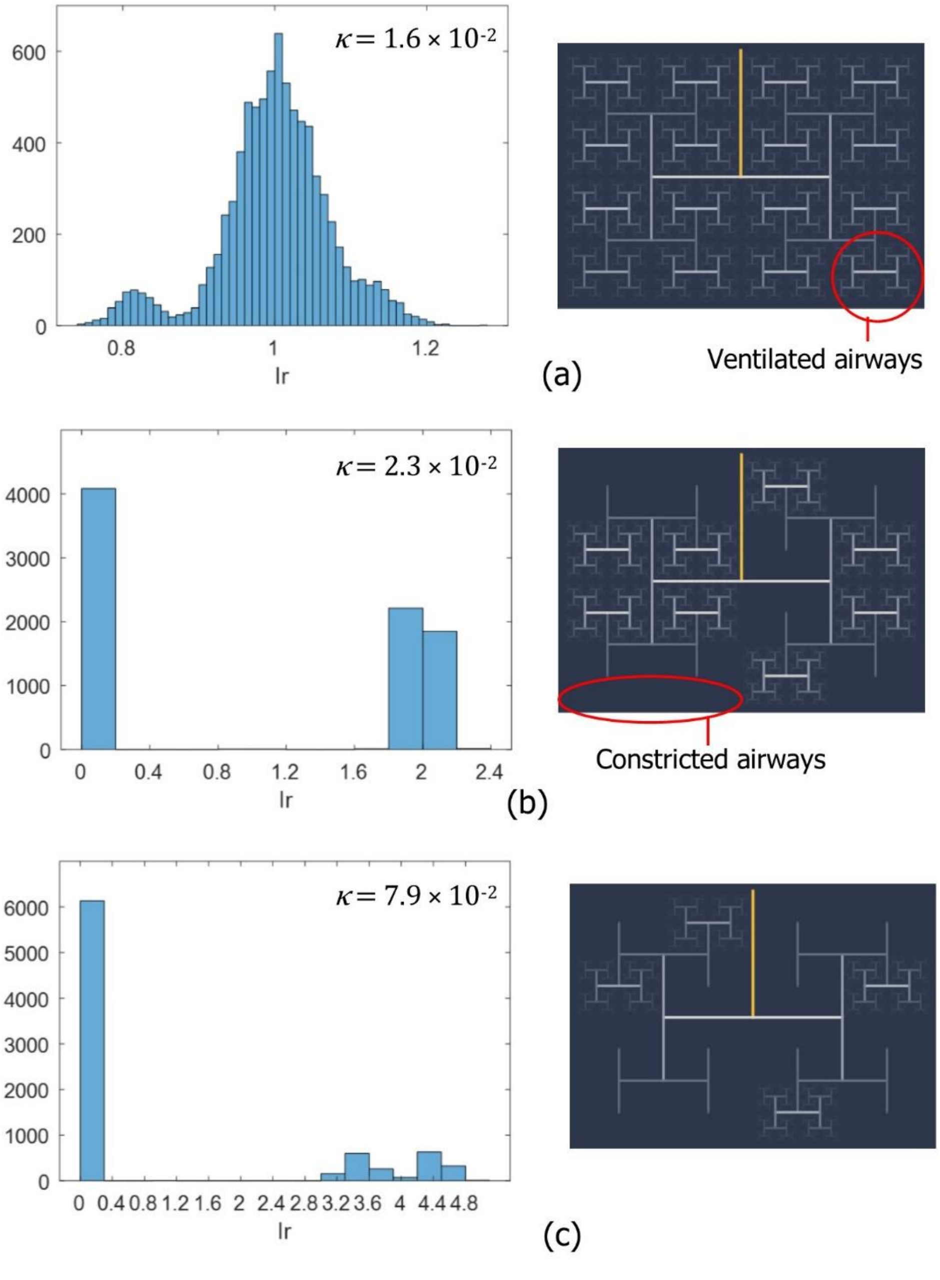

Figure 4.4: Left: histogram of ventilation distribution as flow ratio, Ir, shows polarized distribution. Right: pattern formation of airways. The remaining airways after bronchial constriction are visualized as branches in a Mandelbrot-like tree. Color signifies the conductance, where yellow is the highest. In (b) and (c), many airways in different parts of the tree were constricted. Furthermore, the constriction tends to occur in a cluster.

4.6.2 Sensitivity Analysis

Sensitivity analysis was carried out by running the simulations by perturbing the diameter (D) and length (l) of all airways as in Eq. 4.1. Diameter and length of airways determine the conductivity K_i of the bronchial tree, and small variations were introduced randomly with mean values taken from Ref [83] and variance, σ. Different σ values were used to model aging in bronchial tree, since aging leads to alteration of airway's morphology. Ten simulations were carried out with the same perturbation level (σ values). Fig 4.5 shows the results of ten simulations with $\sigma = 0.01$. The results are presented as network cluster and standard deviation of flow at all edges. As can be seen, both values are the same for all ten trials. Increasing σ to 0.1 also yields the same results for all ten trials. Therefore, it can be concluded that the system is deterministic with the same level of perturbation.

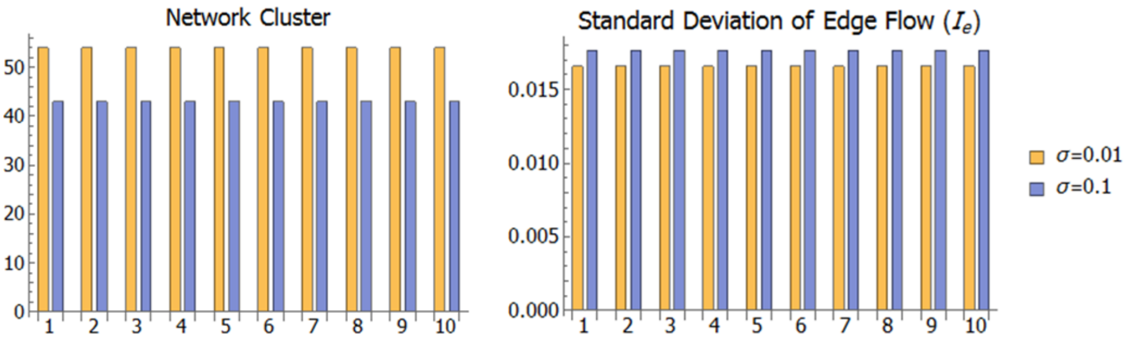

Figure 4.5: Network cluster and standard deviation of edge flow for all edges from ten simulation trials, with two different level of perturbation (σ).

4.6.3 EVOLUTION OF AIRWAY NETWORK COMPLEXITY

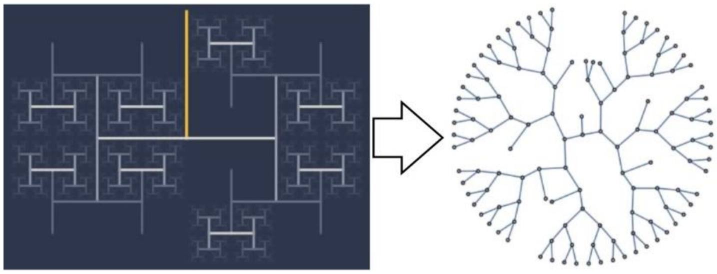

Figure 4.6: The weighted tree network (represented by Mandelbrot-like tree) representing constricted and ventilated airways (Left). An equivalent network can be extracted by removing the constricted airways (Right).

To characterize the airway network according to bronchial constriction progression, we converted the weighted airway networks (which is described by Laplacian matrix L in Eq. 4.2 into a non-weighted network, which we call the simplified network (Fig 4.6). To obtain the simplified network, any edge with weight less than 10^{-8} (i.e., $K_i \leq 10^{-8}$) was removed. We then computed the centrality, Wiener index and the cluster of the airway network as explained in the Method section. The results are plotted against κ which is the control parameter of the adaptation model (Eq. 4.6).

From Fig 4.4, it can be observed that higher κ leads to more constricted airway networks (less ventilated airway). In Fig 4.7(a) for σ =0.01, it can be seen that the constricted airway networks have reduced cluster numbers. Wiener index values are also reduced (Fig 4.7(b)) as expected as airway connectivity reduced with bronchial constriction progression. The topology of the constricted networks can also be distinguished from the less constricted airway network as indicated by Fig 4.7(c). Note the β value for unaltered airway network is ~ 1.85 (lower part of the y-axis in Fig 4.7(c)).

The airway tree is not symmetric, and as explained in Implementation section, this was taken into account with the introduction of variance σ to the diameter and length of the airway. We assume a condition such as aging increases the asymmetries of the airway tree. To simulate this, the variance σ was varied with σ =0.1 and σ =1, and the same computational procedures were carried out as before. In Fig 4.7(a), it can be seen that the more asymmetric airway networks (σ =0.1 and σ=1) have an increased number of clusters as they are more constricted. However, the airway connectivity and network centrality of increased asymmetry cases (σ =0.1 and σ=1) are indistinguishable (Fig 4.7).

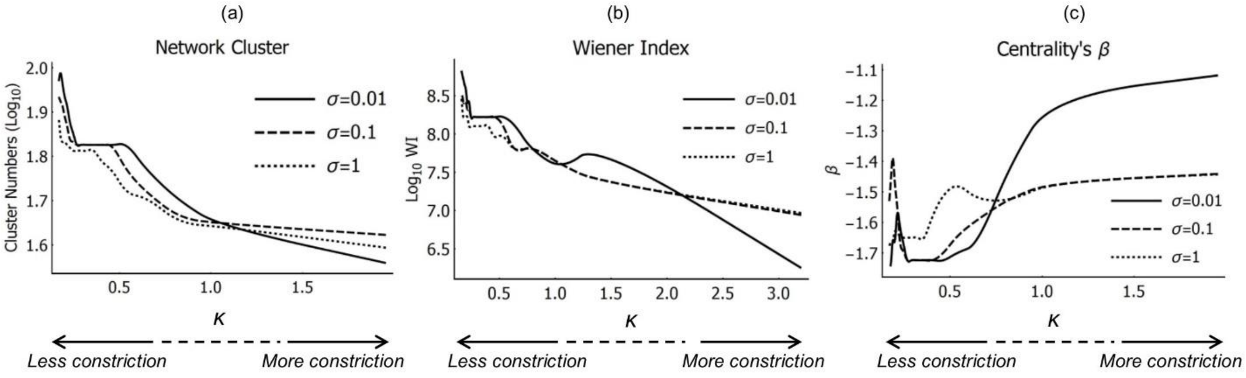

Figure 4.7: Characteristics of airway network with various bronchial constriction and asymmetry level. (a) Cluster numbers declines as airway network becomes more constricted. (b) Wiener index

declines, indicating reduced airway connectivity. (c) β values increased (in negative range) as airway network becomes more constricted, indicating changes in network topology.

4.6.4 RENORMALIZATION AS A MODEL OF BRONCHOCONSTRICTION

We carried out renormalization computation of the unaltered (full) airway tree network. The process is illustrated in Fig 4.3(c). Renormalization of full airway tree takes N_B=38 on average. In this section, we compare bronchial constriction as modeled by network growth (coupled Eq. 4.2 and Eq. 4.6) and network renormalization (CBB algorithm). We extract networks generated with numbers of edges that are the nearest to growth model. In Fig 4.8, we compared the network centrality between the two models. The progression of β values of the two models agreed well indicating similar evolution of network topology for iteration of N_B (renormalization) and κ (network model). Snapshots of the networks are also shown in In Fig 4.8.

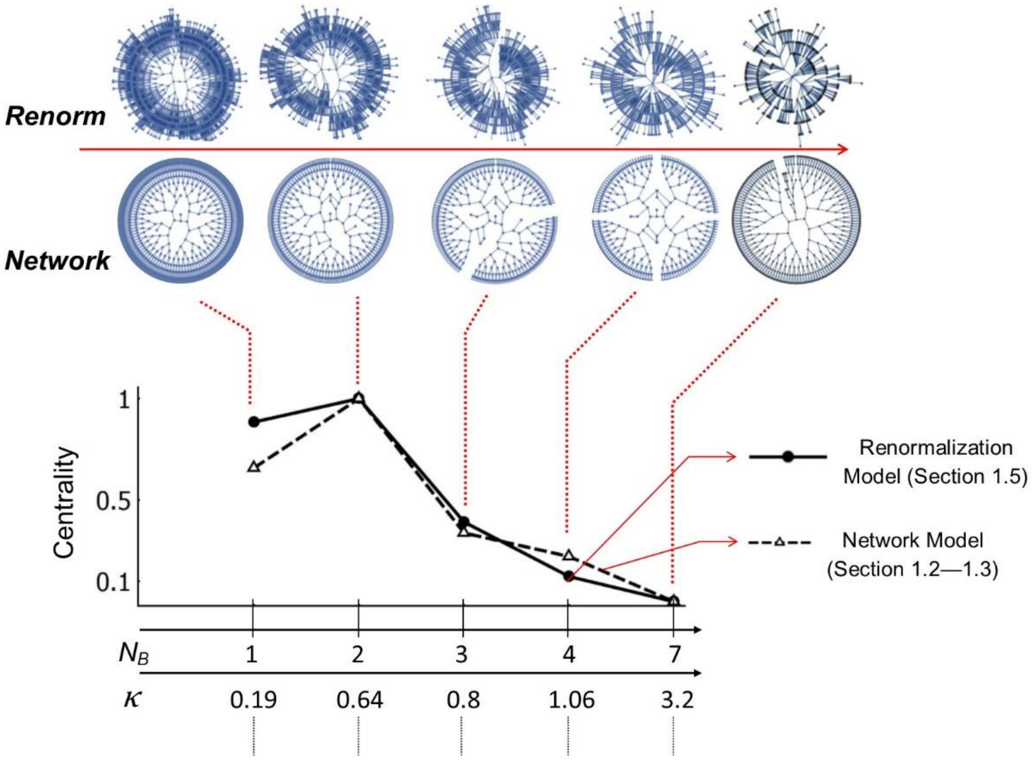

Figure 4.8: Comparison of centrality (β values) of networks generated by renormalization process (*Renorm*) and network growth model (*Network*). Snapshots of the networks are shown on the top. The y-axis values were scaled to range between 0 to 1 to emphasize the progression.

4.7 DISCUSSION

Complexity of the lung structure is known to be altered by disease. The lung airways under asthma and COPD (chronic obstructive lung disease) conditions can be distinguished from each other and healthy lungs by their complexity [90]–[95]. In this study, we incorporated the natural description of the lung as a network to characterize its structural alteration under bronchial constriction. In this study, we demonstrated that the lung with bronchial constriction has reduced Wiener's index and cluster numbers (Fig 4.7). The reduction of network clusters and Wiener index indicates reduction of airway network complexity. Thus, these measures may be used for identification and characterization of lung structure under different diseases. Furthermore, it was shown in another study [87] that less complex networks are typically more vulnerable to an attack that removes nodes and hubs from the network. By referring to our previous results in Fig 4.7, we may also view bronchial constriction is a process that elevates the vulnerability of the airway networks after each "removal of edges" (or airway units). Thus the bronchial constriction is akin to a self-reinforcing process.

We developed a computational model based on a general model of network growth. In this model, higher κ leads to a dynamics that reduce inefficient edges on a network (similar to an optimization process) [23]. As can be seen in Fig 4.4, our results show that higher κ yields highly constricted airway networks. This results may suggest that bronchial constriction, once triggered, may be fundamentally a network optimization process.

In another study [87], another model of network growth based on the concept of renormalization was proposed. In said study, it was argued that network growth and renormalization (coarse-graining) are interrelated concepts. In this study, we compared the renormalization iteration of the airway tree network with the degradation of airway network from the network growth model (Fig 4.8). All three network measures agreed very well for networks (with a similar number of edges) generated by both processes. Thus, the results suggest that bronchial constriction may also share characteristics with network coarse-graining.

These results presented so far may explain bronchial constriction in terms of network dynamics. The bronchial constriction may be analogous to network coarse-graining process that selectively remove edges. However, by removing edges and reducing network complexity, it also increases the vulnerability of the whole network, which in turns exacerbate the disease further. Furthermore, our study demonstrates that it is possible to formulate a framework for modeling disease progression as a network-centric process

4.7.1 LIMITATIONS

The current model is limited to a problem with flux boundary condition (i.e., the flux at each node is known and the potentials are the solution) and resistance as the property of airway. Additional boundary conditions and incorporating airway compliance will enable the model to simulate a broader range of ventilation heterogeneity.

4.8 CONCLUSION

This study investigated bronchial constriction process modeled as adaptive network and quantified their network measures (network clustering, Wiener index and centrality). Lung airways are modeled as a tree network and bronchial constriction as a network adaptation process. Results obtained from the model analysis suggest that network clusters and Wiener index declines by 74% and 71%, respectively, with increasing bronchial constriction. In addition, the airway network centrality under bronchoconstriction can be distinguished from the normal lung conditions. The resulting altered networks show distinguishable characteristics that can potentially be used for identification of airway diseases.

CHAPTER 5

CONCLUSION AND FUTURE WORK

5.1 CONCLUSION

Informatics methods have been applied for analyzing problems of inflammation and bronchoconstriction. An agent-based model was used to model inflammation and wound healing. It reveals that periodic mechanical stimuli (strain) may enhance the robustness of innate immune response. Hence, the inflammation progression may be modulated by mechanical stimuli. The model is able to simulate chronic inflammation by modifying parameters relevant to aging. An informatics framework enables investigation into dominant factors in inflammation. It was revealed that in chronic inflammation, macrophages dominate the information exchange in the system.

The lung is an example of a natural tree network, and bronchoconstriction was modeled as an adaptation process on network domain. This model enables the estimation of airway tree complexity which is important in diagnosing lung disease and investigation of its structure and function. The model is capable of simulating ventilation heterogeneity and estimate the corresponding airway tree complexity.

5.2 FUTURE WORK

The limitation of current inflammation model is reduced redundancy of interactions (e.g., of cells and the cytokines, cell types). In biological systems, the different type of cells have overlapping roles, and so do cytokines. However, in the current model, the overlapping roles are simplified into inflammation exacerbating and inhibiting roles. Some degree of overlapping roles exist in the current model. However, as the degree of overlapping roles decreases, so is the emergent properties of the model. Future research will address the limitations.

To infer information exchange in the inflammation, simulated data were used. However, since it was designed to work with observable data, the method can be directly extended for analyses with real experimental data. This method can be used to determine the dominant factors or agents in a real setting for targeted treatment. This task will be the focus of future research.

The current network model for bronchoconstriction is limited in terms of boundary condition availability and mechanical properties. Future works will be focused to overcome these limitations.

5.3 CONTRIBUTIONS

Although several agent-based models for inflammation exist [10][15][11], the effect of mechanical stimuli as a physical field was not introduced. This study presents a new formulation of agent-based inflammation model driven by mechanical strain and aging factors. The model also provides a general framework for extended analysis, such as cell migrations (demonstrated in Chapter 3) and effect of periodic or fluctuating stimuli to resilience of immune system (demonstrated in Chapter 2, Section 2.3.3). The design of the framework is modular, enabling rapid adaptation to other problems with similar interacting events and units.

Currently, there is a lack of computational framework for analyzing inflammation as information processing system, despite the importance of signal transduction in cells migration [54], diseases [49][52] and ultimately determining the fate of inflammations. In addition, complex process such as inflammation involves interaction between many events that determine its outcome. Therefore, a method to quantify information exchange between events are needed. In Chapter 3, method to quantify information exchange is introduced to fill the knowledge gap. Application of the method is demonstrated in Chapter 3 where dominant agents in (simulated) normal and chronic inflammation (inflammaging) were identified. In the future, the method can be extended to infer dominant events (such as cytokine release, fibrosis) given a case of inflammation (e.g., chronic or normal inflammation). Identifying dominant events or factors will provide automated inference of targets to inhibit or modulate the outcome of inflammation (e.g., inhibit cytokine release, inhibit macrophage migration).

The lung is natural network and its morphology determines its function. However, there is a lack of graph-based computational framework for lung dynamics. In Chapter 4, a graph-based approach for simulating lung morphological changes due to bronchoconstriction is introduced. The graph-based approach naturally provide a way to estimate reduction of morphological complexity in the lung due to airway constriction. In the future, this approach can be extended to analyze other problems that can be formulated as a network/graph domain.

The reports from this study have been published in Refs [66], [96] [97], [98] and [99].

5.4 ACKNOWLEDGEMENT

The authors thank the U. S. National Science Foundation for sponsoring the research through an NSF grant CMMI-1430379.

REFERENCES

[1] P. Hunter, “The inflammation theory of disease,” *EMBO Rep.*, vol. 13, no. 11, pp. 968–970, 2012.

[2] M. G. Netea, F. Balkwill, M. Chonchol, F. Cominelli, M. Y. Donath, E. J. Giamarellos-Bourboulis, D. Golenbock, M. S. Gresnigt, M. T. Heneka, H. M. Hoffman, and others, “A guiding map for inflammation,” *Nat. Immunol.*, vol. 18, no. 8, p. 826, 2017.

[3] J. M. Blander, R. S. Longman, I. D. Iliev, G. F. Sonnenberg, and D. Artis, “Regulation of inflammation by microbiota interactions with the host,” *Nat. Immunol.*, vol. 18, no. 8, p. 851, 2017.

[4] P. J. Barnes, “Immunology of asthma and chronic obstructive pulmonary disease,” *Nat. Rev. Immunol.*, vol. 8, no. 3, p. 183, 2008.

[5] J. M. Graham, B. P. Ayati, L. Ding, P. S. Ramakrishnan, and J. A. Martin, “Reaction-Diffusion-Delay Model for EPO/TNF-α Interaction in Articular Cartilage Lesion Abatement,” 2011.

[6] Y. Vodovotz, G. Constantine, J. Rubin, M. Csete, E. O. Voit, and G. An, “Mechanistic simulations of inflammation: Current state and future prospects,” *Math. Biosci.*, vol. 217, no. 1, pp. 1–10, 2009.

[7] R. T. Tranquillo and J. D. Murray, “Continuum model of fibroblast-driven wound contraction: Inflammation-mediation,” *J. Theor. Biol.*, vol. 158, no. 2, pp. 135–172, Sep.

1992.

[8] E. Javierre, P. Moreo, M. Doblaré, and J. M. García-Aznar, “Numerical modeling of a mechano-chemical theory for wound contraction analysis,” *Int. J. Solids Struct.*, vol. 46, no. 20, pp. 3597–3606, 2009.

[9] B. Chopard and M. Droz, *Cellular Automata Modeling of Physical Systems*, Cambridge,. Cambridge University Press, 1998.

[10] A. Reynolds, K. Koombua, R. M. Pidaparti, and K. R. Ward, “Cellular Automata Modeling of Pulmonary Inflammation,” vol. 9, no. 2, pp. 141–156, 2012.

[11] B. N. Brown, I. M. Price, F. R. Toapanta, D. R. DeAlmeida, C. A. Wiley, T. M. Ross, T. D. Oury, and Y. Vodovotz, “An agent-based model of inflammation and fibrosis following particulate exposure in the lung.,” *Math. Biosci.*, vol. 231, no. 2, pp. 186–96, Jun. 2011.

[12] G. B. Ermentrout and L. Edelstein-Keshet, “Cellular automata approaches to biological modeling.,” *J. Theor. Biol.*, vol. 160, no. 1, pp. 97–133, Jan. 1993.

[13] D. Alemani, F. Pappalardo, M. Pennisi, S. Motta, and V. Brusic, “Combining cellular automata and Lattice Boltzmann method to model multiscale avascular tumor growth coupled with nutrient diffusion and immune competition.,” *J. Immunol. Methods*, vol. 376, no. 1–2, pp. 55–68, Feb. 2012.

[14] M. Precharattana and W. Triampo, “Modeling dynamics of HIV infected cells using stochastic cellular automaton,” *Phys. A Stat. Mech. its Appl.*, vol. 407, pp. 303–311, Aug. 2014.

[15] J. Dutta-Moscato, A. Solovyev, Q. Mi, T. Nishikawa, A. Soto-Gutierrez, I. J. Fox, and Y.

Vodovotz, “A Multiscale Agent-Based in silico Model of Liver Fibrosis Progression.,” *Front. Bioeng. Biotechnol.*, vol. 2, no. May, p. 18, 2014.

[16] A. Rao, E. Huynh, T. J. Royston, A. Kornblith, and S. Roy, “Acoustic Methods for Pulmonary Diagnosis,” *IEEE Rev. Biomed. Eng.*, vol. 12, pp. 221–239, 2019.

[17] M. Eskandari, W. G. Kuschner, and E. Kuhl, “Patient-Specific Airway Wall Remodeling in Chronic Lung Disease,” *Ann. Biomed. Eng.*, 2015.

[18] W. A. Wall and T. Rabczuk, “Fluid-structure interaction in lower airways of CT-based lung geometries,” *Int. J. Numer. Methods Fluids*, no. October 2007, pp. 653–675, 2008.

[19] M. Weilenmann, L. Krämer, P. Faist, and R. Renner, “Axiomatic relation between thermodynamic and information-theoretic entropies,” *arXiv*, vol. 260601, no. Proposition 1, pp. 1–20, 2015.

[20] D. Blokh and I. Stambler, “The application of information theory for the research of aging and aging-related diseases,” *Prog. Neurobiol.*, 2016.

[21] T. McGrath, N. S. Jones, P. R. ten Wolde, and T. E. Ouldridge, “Biochemical Machines for the Interconversion of Mutual Information and Work,” *Phys. Rev. Lett.*, vol. 118, no. 2, p. 028101, 2017.

[22] L. J. Grady and J. R. Polimeni, *Discrete Calculus: Applied Analysis on Graphs for Computational Science*. Springer London, 2010.

[23] H. Ronellenfitsch and E. Katifori, “Global optimization, local adaptation and the role of growth in distribution networks,” *Phys. Rev. Lett.*, vol. 138301, no. SEPTEMBER, pp. 1–5, 2016.

[24] L. Mari, R. Casagrandi, E. Bertuzzo, A. Rinaldo, and M. Gatto, “Metapopulation persistence and species spread in river networks,” *Ecol. Lett.*, vol. 17, no. 4, pp. 426–434, 2014.

[25] C. Brelsford, T. Martin, J. Hand, and L. M. A. Bettencourt, “Toward cities without slums: Topology and the spatial evolution of neighborhoods,” *Sci. Adv.*, vol. 4, no. 8, 2018.

[26] L. Tremblay and A. Slutsky, “Ventilator-induced injury: from barotrauma to biotrauma,” *Proc Assoc Am Physicians*, vol. 110, pp. 482–488, 1998.

[27] F. J. J. Halbertsma, M. Vaneker, G. J. Scheffer, and J. G. Van Der Hoeven, “Cytokines and biotrauma in ventilator-induced lung injury: a critical review of the literature,” *J. Med.*, vol. 63, no. 10, pp. 382–392, 2005.

[28] C. K. Wong and M. C. Easton, “An Efficient Method for Weighted Sampling Without Replacement,” *SIAM J. Comput.*, vol. 9, no. 1, pp. 111–113, 1980.

[29] P. C. Rath and B. B. Aggarwal, “TNF-induced signaling in apoptosis.,” *J. Clin. Immunol.*, vol. 19, no. 6, pp. 350–364, 1999.

[30] A. Kelso, “Cytokines: Principles and prospects,” *Immunol. Cell Biol.*, vol. 76, no. 4, pp. 300–317, 1998.

[31] S. Uhlig and U. Uhlig, “Pharmacological interventions in ventilator-induced lung injury.,” *Trends Pharmacol. Sci.*, vol. 25, no. 11, pp. 592–600, Nov. 2004.

[32] J. Nam, B. D. Aguda, B. Rath, and S. Agarwal, “Biomechanical thresholds regulate inflammation through the NF-κB pathway: Experiments and modeling,” *PLoS One*, vol. 4, no. 4, 2009.

[33] D. E. Sullivan, M. Ferris, H. Nguyen, E. Abboud, and R. Arnold, “TNF-α induces TGFβ1 -expression in lung fibroblasts at the transcriptional level via AP-1 activation,” *J Cell Mol Med*, vol. 13, no. 8B, pp. 1866–1876, 2010.

[34] M. B. Witte and A. Barbul, “GENERAL PRINCIPLES OF WOUND HEALING,” *Surg. Clin. North Am.*, vol. 77, no. 3, pp. 509–528, 1997.

[35] S. E. Sinclair, R. C. Molthen, S. T. Haworth, C. A. Dawson, and C. M. Waters, “Airway strain during mechanical ventilation in an intact animal model,” *Am. J. Respir. Crit. Care Med.*, vol. 176, no. 8, pp. 786–794, 2007.

[36] H. Wokalek and H. Ruh, “Time Course of Wound Healing,” *J. Biomater. Appl.*, vol. 5, no. 4, pp. 337–362, 1991.

[37] J. M. Davidson, “Wound Repair,” in *Inflammation : Basic Principles and Clinical Correlates*, R. S. John I Gallin Ira M Goldstein, Ed. New York: Raven Press, 1992, pp. 806–819.

[38] F. J. Pixley, “Macrophage Migration and Its Regulation by CSF-1,” *Int. J. Cell Biol.*, vol. 2012, no. 501962, pp. 1–12, 2012.

[39] F. Krombach, S. Münzing, A. M. Allmeling, J. T. Gerlach, J. Behr, and M. Dörger, “Cell size of alveolar macrophages: an interspecies comparison.,” *Environ. Health Perspect.*, vol. 105 Suppl, no. September, pp. 1261–1263, 1997.

[40] R. A. F. Jr., “Cytometrics,” in *Nanomedicine, Volume I: Basic Capabilities*, Georgetown, TX: Landes Bioscience, 1999, p. 247.

[41] S. C. Gnyawali, K. G. Barki, S. S. Mathew-Steiner, S. Dixith, D. Vanzant, J. Kim, J. L.

Dickerson, S. Datta, H. Powell, S. Roy, V. Bergdall, and C. K. Sen, “High-Resolution Harmonics Ultrasound Imaging for Non-Invasive Characterization of Wound Healing in a Pre-Clinical Swine Model,” *PLoS One*, vol. 10, no. 3, pp. 1–19, 2015.

[42] Gierer and Meinhardt, “A Theory of Biological Pattern Formation,” *Kybernetik*, vol. 12. pp. 30–39, 1972.

[43] N. E. Vlahakis, M. A. Schroeder, A. H. Limper, and R. D. Hubmayr, “Stretch induces cytokine release by alveolar epithelial cells in vitro,” *Am. J. Physology*, vol. 277, pp. 167–173, 1999.

[44] H. Yamamoto, H. Teramoto, K. Uetani, K. Igawa, and E. Shimizu, “Cyclic stretch upregulates interleukin-8 and transforming growth factor-??1 production through a protein kinase C-dependent pathway in alveolar epithelial cells,” *Respirology*, vol. 7, no. 2, pp. 103–109, 2002.

[45] P. C. Rath and B. B. Aggarwal, “TNF-induced signaling in apoptosis,” *J. Clin. Immunol.*, vol. 19, no. 6, pp. 350–364, 1999.

[46] H. Mulller-Redetzky, J. Lienau, N. Suttorp, and M. Witzenrath, “Therapeutic strategies in pneumonia: Going beyond antibiotics,” *Eur. Respir. Rev.*, vol. 24, no. 137, pp. 516–524, 2015.

[47] Z. Frankenstein, U. Alon, and I. R. Cohen, “The immune-body cytokine network defines a social architecture of cell interactions,” *Biol. Direct*, vol. 1, no. 1, p. 32, Oct. 2006.

[48] A. Rivera, M. C. Siracusa, G. S. Yap, and W. C. Gause, “Innate cell communication kick-starts pathogen-specific immunity,” *Nat. Immunol.*, vol. 17, pp. 356–363, 2016.

[49] G. A. Garden and A. R. LaSpada, “Intercellular (Mis)communication in Neurodegenerative Disease,” *Neuron*, vol. 73, no. 5, pp. 886–901, 2012.

[50] P. Aghasafari, U. George, and R. Pidaparti, “A review of inflammatory mechanism in airway diseases,” *Inflamm. Res.*, vol. 68, no. 1, pp. 59–74, 2019.

[51] G. S. Martin, “Cell signaling and cancer,” *Cancer Cell*, vol. 4, no. 3, pp. 167–174, 2003.

[52] T. Peng, H. Peng, D. S. Choi, J. Su, C. C. (Jeff) Chang, and X. Zhou, “Modeling Cell--Cell Interactions in Regulating Multiple Myeloma Initiating Cell Fate,” *IEEE J. Biomed. Heal. Informatics*, vol. 18, no. 2, pp. 484–491, Mar. 2014.

[53] J. C. Rieckmann, R. Geiger, D. Hornburg, T. Wolf, K. Kveler, D. Jarrossay, F. Sallusto, S. S. Shen-Orr, A. Lanzavecchia, M. Mann, and F. Meissner, “Social network architecture of human immune cells unveiled by quantitative proteomics,” *Nat. Immunol.*, vol. 18, pp. 583–593, Mar. 2017.

[54] T. Frank and S. Tay, “Automated co-culture system for spatiotemporal analysis of cell-to-cell communication,” *Lab Chip*, vol. 15, no. 10, pp. 2192–2200, 2015.

[55] C. López-Otín, M. A. Blasco, L. Partridge, M. Serrano, and G. Kroemer, “The Hallmarks of Aging,” *Cell*, vol. 153, no. 6, pp. 1194–1217, 2013.

[56] S. Vedel, S. s Tay, D. M. Johnston, H. Bruus, and S. R. Quake, “Migration of cells in a social context,” *Proc. Natl. Acad. Sci.*, vol. 110, no. 1, pp. 129–134, 2013.

[57] W.-J. Rappel, “Cell-cell communication during collective migration,” *Proceedings of the National Academy of Sciences*, vol. 113, no. 6. National Academy of Sciences, pp. 1471–1473, 2016.

[58] B. Sun, J. Lembong, V. Normand, M. Rogers, and H. A. Stone, “Spatial-temporal dynamics of collective chemosensing,” *Proc. Natl. Acad. Sci.*, vol. 109, no. 20, pp. 7753–7758, 2012.

[59] H. Youk and W. A. Lim, “Secreting and Sensing the Same Molecule Allows Cells to Achieve Versatile Social Behaviors,” *Science (80-.).*, vol. 343, no. 6171, 2014.

[60] V. V Abhyankar and D. J. Beebe, “Spatiotemporal Micropatterning of Cells on Arbitrary Substrates,” *Anal. Chem.*, vol. 79, no. 11, pp. 4066–4073, 2007.

[61] J. Escribano, R. Sunyer, M. T. Sánchez, X. Trepat, P. Roca-Cusachs, and J. M. García-Aznar, “A hybrid computational model for collective cell durotaxis,” *Biomech. Model. Mechanobiol.*, vol. 17, no. 4, pp. 1037–1052, Aug. 2018.

[62] F. J. Vermolen and A. Gefen, “A semi-stochastic cell-based formalism to model the dynamics of migration of cells in colonies,” *Biomech. Model. Mechanobiol.*, vol. 11, no. 1, pp. 183–195, Jan. 2012.

[63] N. Kuzmic, T. Moore, D. Devadas, and E. W. K. Young, “Modelling of endothelial cell migration and angiogenesis in microfluidic cell culture systems,” *Biomech. Model. Mechanobiol.*, Jan. 2019.

[64] A. Moure and H. Gomez, “Three-dimensional simulation of obstacle-mediated chemotaxis,” *Biomech. Model. Mechanobiol.*, vol. 17, no. 5, pp. 1243–1268, Oct. 2018.

[65] S. S. Shishvan, A. Vigliotti, and V. S. Deshpande, “The homeostatic ensemble for cells,” *Biomech. Model. Mechanobiol.*, vol. 17, no. 6, pp. 1631–1662, Dec. 2018.

[66] I. Ibrahim, S. V. Oruganti, and R. Pidaparti, “Simulation of Healing Threshold in Strain-Induced Inflammation through a Discrete Informatics Model,” *IEEE J. Biomed. Heal.*

Informatics, vol. 2194, no. c, pp. 1–1, 2017.

[67] P. Aghasafari, I. Bin M. Ibrahim, and R. Pidaparti, “Strain-induced inflammation in pulmonary alveolar tissue due to mechanical ventilation,” *Biomech. Model. Mechanobiol.*, vol. 16, no. 4, pp. 1103–1118, 2017.

[68] M. Poujade, E. Grasland-Mongrain, A. Hertzog, J. Jouanneau, P. Chavrier, B. Ladoux, A. Buguin, and P. Silberzan, “Collective migration of an epithelial monolayer in response to a model wound,” *Proc. Natl. Acad. Sci.*, vol. 104, no. 41, pp. 15988–15993, 2007.

[69] S. Butail, V. Mwaffo, and M. Porfiri, “Model-free information-theoretic approach to infer leadership in pairs of zebrafish,” *Phys. Rev. E*, vol. 93, no. 4, p. 42411, Apr. 2016.

[70] S. Frenzel and B. Pompe, “Partial Mutual Information for Coupling Analysis of Multivariate Time Series,” *Phys. Rev. Lett.*, vol. 99, no. 20, p. 204101, Nov. 2007.

[71] S. Guo and L. A. DiPietro, “Factors Affecting Wound Healing,” *J. Dent. Res.*, vol. 89, no. 3, pp. 219–229, 2010.

[72] A. Gosain and L. A. DiPietro, “Aging and Wound Healing,” *World J. Surg.*, vol. 28, no. 3, pp. 321–326, Mar. 2004.

[73] C. Castelo-Branco and I. Soveral, “The immune system and aging: a review,” *Gynecol. Endocrinol.*, vol. 30, no. 1, pp. 16–22, 2014.

[74] L. Hecker, N. J. Logsdon, D. Kurundkar, A. Kurundkar, K. Bernard, T. Hock, E. Meldrum, Y. Y. Sanders, and V. J. Thannickal, “Reversal of Persistent Fibrosis in Aging by Targeting Nox4-Nrf2 Redox Imbalance,” *Sci. Transl. Med.*, vol. 6, no. 231, p. 231ra47--231ra47, 2014.

[75] G. Raghu, D. Weycker, J. Edelsberg, W. Z. Bradford, and G. Oster, “Incidence and Prevalence of Idiopathic Pulmonary Fibrosis,” *Am. J. Respir. Crit. Care Med.*, vol. 174, no. 7, pp. 810–816, 2006.

[76] T. Padmore, C. Stark, L. A. Turkevich, and J. A. Champion, “Quantitative analysis of the role of fiber length on phagocytosis and inflammatory response by alveolar macrophages,” *Biochim. Biophys. Acta - Gen. Subj.*, vol. 1861, no. 2, pp. 58–67, 2017.

[77] F. Guo, P. Li, J. B. French, Z. Mao, H. Zhao, S. Li, N. Nama, J. R. Fick, S. J. Benkovic, and T. J. Huang, “Controlling cell-cell interactions using surface acoustic waves,” *Proc. Natl. Acad. Sci.*, vol. 112, no. 1, pp. 43–48, 2015.

[78] E. E. Hui and S. N. Bhatia, “Micromechanical control of cell-cell interactions,” *Proc. Natl. Acad. Sci.*, vol. 104, no. 14, pp. 5722–5726, 2007.

[79] J. G. Venegas, T. Winkler, G. Musch, M. F. V. Melo, D. Layfield, N. Tgavalekos, A. J. Fischman, R. J. Callahan, G. Bellani, and R. S. Harris, “Self-organized patchiness in asthma as a prelude to catastrophic shifts,” *Nature*, vol. 434, no. April, pp. 777–782, 2005.

[80] T. Winkler, “Airway Transmural Pressures in an Airway Tree During Bronchoconstriction in Asthma,” *J. Eng. Sci. Med. Diagnostics Ther.*, vol. 2, no. 1, p. 11005, 2019.

[81] M. Kim, R. Bordas, W. Vos, R. A. Hartley, C. E. Brightling, D. Kay, V. Grau, and K. S. Burrowes, “Dynamic flow characteristics in normal and asthmatic lungs,” *Int. j. numer. method. biomed. eng.*, vol. 31, no. 12, 2015.

[82] T. J. Pedley, R. C. Schroter, and M. F. Sudlow, “The prediction of pressure drop and variation of resistance within the human bronchial airways,” *Respir. Physiol.*, vol. 9, no.

October 1969, pp. 387–405, 1970.

[83] B. Maury, “Data,” in *The Respiratory System in Equations*, Milano: Springer Milan, 2013, pp. 215–224.

[84] T. Winkler and J. G. Venegas, “Complex airway behavior and paradoxical responses to bronchoprovocation,” *J. Appl. Physiol.*, vol. 103, no. 2, p. 655, 2007.

[85] J. M. Fletcher and T. Wennekers, “From Structure to Activity: Using Centrality Measures to Predict Neuronal Activity,” *Int. J. Neural Syst.*, vol. 28, no. 02, p. 1750013, 2018.

[86] V. D. Blondel, J.-L. Guillaume, R. Lambiotte, and E. Lefebvre, “Fast unfolding of communities in large networks,” *J. Stat. Mech. Theory Exp.*, vol. 2008, no. 10, p. P10008, Oct. 2008.

[87] C. Song, S. Havlin, and H. A. Makse, “Origins of fractality in the growth of complex networks,” *Nat. Phys.*, vol. 2, pp. 275–281, 2006.

[88] N. G. Van Kampen, *Stochastic processes in physics and chemistry*, vol. 1. Elsevier, 1992.

[89] C. Song, L. K. Gallos, S. Havlin, and H. A. Makse, “How to calculate the fractal dimension of a complex network: the box covering algorithm,” *J. Stat. Mech. Theory Exp.*, vol. 2007, no. 03, pp. P03006--P03006, Mar. 2007.

[90] J. Veiga, R. C. P. Faria, G. P. Esteves, A. J. Lopes, J. M. Jansen, and P. L. Melo, “Approximate entropy as a measure of the airflow pattern complexity in asthma,” in *2010 Annual International Conference of the IEEE Engineering in Medicine and Biology*, 2010, pp. 2463–2466.

[91] R. A. Hartley, B. L. Barker, C. Newby, M. Pakkal, S. Baldi, R. Kajekar, R. Kay, M. Laurencin, R. P. Marshall, A. R. Sousa, H. Parmar, S. Siddiqui, S. Gupta, and C. E. Brightling, "Relationship between lung function and quantitative computed tomographic parameters of airway remodeling, air trapping, and emphysema in patients with asthma and chronic obstructive pulmonary disease: A single-center study," *J. Allergy Clin. Immunol.*, vol. 137, no. 5, p. 1413–1422.e12, 2016.

[92] S. R. Boser, H. Park, S. F. Perry, M. G. Ménache, and F. H. Y. Green, "Fractal Geometry of Airway Remodeling in Human Asthma," *Am. J. Respir. Crit. Care Med.*, vol. 172, no. 7, pp. 817–823, 2005.

[93] S. Bodduluri, A. S. K. Puliyakote, S. E. Gerard, J. M. Reinhardt, E. A. Hoffman, J. D. N. Jr., H. P. Nath, M. K. Han, G. R. Washko, R. S. J. Estépar, M. T. Dransfield, S. P. Bhatt, and Copdg. Investigators, "Airway fractal dimension predicts respiratory morbidity and mortality in COPD," *J. Clin. Invest.*, vol. 128, no. 12, pp. 5374–5382, 2018.

[94] N. Tanabe, S. Muro, S. Sato, T. Oguma, A. Sato, and T. Hirai, "Fractal analysis of low attenuation clusters on computed tomography in chronic obstructive pulmonary disease," *BMC Pulm. Med.*, vol. 18, no. 1, p. 144, Aug. 2018.

[95] D. Copot, R. De Keyser, E. Derom, and C. Ionescu, "Structural changes in the COPD lung and related heterogeneity," *PLoS One*, vol. 12, no. 5, pp. 1–21, 2017.

[96] P. Aghasafari, I. Bin M. Ibrahim, and R. Pidaparti, "Strain-induced inflammation in pulmonary alveolar tissue due to mechanical ventilation," *Biomech. Model. Mechanobiol.*, vol. 16, no. 4, pp. 1103–1118, Aug. 2017.

[97] I. B. M. Ibrahim and R. Pidaparti, “Influence of Pathogens and Mechanical Stimuli in Inflammation,” *Bioengineering*, vol. 6, no. 2, 2019.

[98] I. Ibrahim, P. Aghasafari, and R. Pidaparti, “Transient Mechanical Response of Lung Airway Tissue during Mechanical Ventilation,” *Bioengineering*, vol. 3, no. 1, p. 4, 2016.

[99] I. Bin M. Ibrahim, R. M. Pidaparti, and K. R. Ward, “Evaluation of Ventilation-Induced Lung Inflammation Through Multi-Scale Simulations,” *IEEE J. Transl. Eng. Heal. Med.*, vol. 6, pp. 1–7, 2018.

APPENDIX A

SUPPLEMENTAL MATERIALS FOR CHAPTER 2

SIMULATION OF WOUND HEALING AND CELL'S DYNAMICS UNDER STRAIN-INDUCED INFLAMMATION

7.1 PSEUDOCODE

```
Begin
    Parameters Initialization (Table 2.1 and Table 2.2)
    Matrix Initialization for Epithelial Cells Grid
    Matrix Initialization for TNF
    Matrix Initialization for TGF
    Matrix Initialization for Elastic Grid
    Matrix Initialization for Motile Cells and Fibrosis
    time= 1;
    While time $\leq$ total time
        Execute Eq. 2.11 (Motile Cell Activation)
        Execute Eq. 2.16 (Cytokine Diffusion)
        Execute Eq. 2.12 and Eq. 2.13 (Cytokine release)
```

```
        Epithelial Cells Subroutine:

        Execute Eq. 2.5 (Apoptosis and/or healing)

        Execute Eq. 2.6 (Fibrosis)

        Execute Eq. 2.9 and Eq. 2.10 (Motile cells migration)

        If $t_{im}$ (motile cell life time) of motile cell (i,j) $\leq 0$

            Reinitialize at random (i,j) location

        End

        time = time +1;

    End (While)

End
```

7.2 MATLAB IMPLEMENTATION

7.2.1 MAIN FUNCTION

```
function CAstartcase
format compact

fname= input('enter file name to store sim data: ','s');

%grid creation
tissueSz=[100 100];
%---------------------------------------
% Parameters
global totalIters; totalIters=1000;
global totaltrial; totaltrial=1;
% global fname;
%___________________Stochastic Parameters_____________________________
%-----------------Beta Distribution parameters, (alpha, beta) -------------
%Macrophages Activation
abia=[5,1];
%TNf and TGF releases
```

```
abtnf=[1,3];
abtgf=[2,1];
% Epithelial apopotosis
abapop=[5,1];

%population variance
musig=[0.5,0.25];

%---------------fixed cells (epithelial)
% epthMat=zeros(tissueSz);
%mitosis rate
mt=5;

%-----------------------------diffusing grid
% Diffusion-degradation constants: (diffusity, degradation)
% DKtnf=[0.07, 1e-3];  %pro-inflammatory/activator ~ TNF
% DKtgf=[0.1, 1e-5];   %anti-inflammatorty/inhibitor ~ TGF
DKtnf=[0.1, 1e-3];  %pro-inflammatory/activator ~ TNF
DKtgf=[0.07, 1e-5];   %anti-inflammatorty/inhibitor ~ TGF

%---------------physical grid
                                 wn=[2];   %number of oscillation in sinusoidal
wave
                                Amp=0.5; %amplitude
                               strtype=4;

Aact=1;
%------------------------------mobile cells: cells with motility
%nstate: number of type of states, state and age
%sval: the values of states (initial)
%mcr=macrophages, fbr= fibroblasts
%immune cell's velocity
mcr_v=3;
fbr_v=3;
%mobile cell's cytokines sensitivity (affect locomotion)
nrn=10;

%immune cell repopulation rate
tpoplc=5;
%immune cell's age
macrLife= 20;
fbrLife= 20;
%immune cells average population
nMacroph= 25;
nFibrob= 25;

%additional
%fibroblast differentiating time
td=5;
%collagen density-increase time
% tclg=5;
tclg=10;

%initial/starting state
```

```
sval1=[1 macrLife];
sval2=[11 fbrLife];
%range of state of immune cells
%macrophages
strange_M=[1 10];
%fibroblasts
strange_F=[11 20];
%immune cell's grid contain: state and age
nstate=2;
tpopl=tpoplc;

%~~~~~~~~~~~~~~~~~~~~~~~~~~~~~~~~~~~```````````````````````````````````````
ncase=length(wn);
for cs=1:ncase
for trial=1:totaltrial
     fprintf('\t\t\t\t\t\t\t\t\t\t\t trial: %i \n',trial)
[CA]=iterate(tissueSz,abia,abtnf,abtgf,abapop,musig,mt,...
    DKtnf,DKtgf,Amp,strtype,Aact,mcr_v,fbr_v,nrn,tpoplc,...

nMacroph,nFibrob,td,tclg,sval1,sval2,strange_M,strange_F,nstate,tpopl,wn(cs))
;

fname1= strcat(fname,'_tr',num2str(trial),'_wn',num2str(wn(cs)));
save( fname1, 'CA','-v7.3' )
clear CA

end
end

end   %end function
```

7.2.2 SUBROUTINE ITERATE (MAIN CA LOOP)

```
function [CA]=iterate(tissueSz,abia,abtnf,abtgf,abapop,musig,mt,...
    DKtnf,DKtgf,Amp,strtype,Aact,mcr_v,fbr_v,nrn,tpoplc,...
    nMacroph,nFibrob,td,tclg,sval1,sval2,strange_M,strange_F,nstate,tpopl,wn)

% % Initialization
% format compact
%note: interchangeable in the notes:
%mobile/motile cells & immune cells
%taxis, locomotion, movement
global totalIters;

%__________________________________________________________________________
%--------------------------------------------------------------------------
%cell's array indexing
fixed=1; mobile=2; diff=3; phys=4;
%__________________________________________________________________________
%--------------------------------------------------------------------------
for tidx=1:totalIters
CA{tidx,fixed,1}=zeros(tissueSz);
```

```
CA{tidx,mobile,1}=zeros(tissueSz);
CA{tidx,mobile,2}=zeros(tissueSz);
CA{tidx,mobile,3}=zeros(tissueSz);
CA{tidx,diff,1}=zeros(tissueSz);
CA{tidx,diff,2}=zeros(tissueSz);
CA{tidx,phys,1}=zeros(tissueSz);
end

%store elastic field grid
% wn=1;   %number of oscillation in sinusoidal wave
for ti=1:totalIters
% [epthStrain]= straindist(tissueSz,Amp,strtype);
%sinusoidal increase of strain
% Ampt=abs((Amp*sin(pi*wn*ti/totalIters))+ Amp/2);
Ampt=abs((Amp*sin(pi*wn*ti/totalIters)));
CA{ti ,phys,1}= straindist(tissueSz,Ampt,strtype);
end

tic; %start to count comp time
cta=zeros(1,1);

epthMat=zeros(tissueSz);
%init immune cell's grid
for istate=1:nstate
motile(:,:,istate)= zeros(tissueSz);
end
%populate macrophages
[motile]= populate(motile,sval1,strange_M,nMacroph,musig);
%populate fibroblast
[motile]= populate(motile,sval2,strange_F,nFibrob,musig);

%---------------diffusing cells
TNFmat=zeros(tissueSz); TGFmat=zeros(tissueSz);

%      rng('shuffle');
%start simulation time
for t=1:totalIters
 fprintf('\t\t\t\t\t\t\t\t\t\t    sim time: %i \n',t)
%store sim data each time step
CA{t,fixed,1}=epthMat;
CA{t,mobile,1}=motile;
CA{t,diff,1}=TNFmat;
CA{t,diff,2}=TGFmat;
%specific output
%macrophages only
mtemp=motile(:,:,1);mtemp(mtemp==11 | mtemp==-1)=0;
CA{t,mobile,2}=mtemp;
%fibroblast only
mtemp=motile(:,:,1); mtemp(mtemp==1 | mtemp==2)=0;
CA{t,mobile,3}=mtemp;

%---------------------Rules----------------------------------------------
%---------------------main update----------------------------------------
% macrophage activation
```

```
disp('activating macrophages')
 [motile(:,:,1)]=inact2act(CA{t,mobile,1}(:,:,1),CA{t ,phys,1},Aact,abia);
% [motile(:,:,1)]=inact2act(CA{t,mobile,1}(:,:,1),epthStrain,Aact,abia);

 %cytokines releases and diffuse - add reaction diffusion here
fprintf('\t\t\t\t\t diffusing cytokines \n')
 [TNFmat,TGFmat]=
cytodiff(CA{t,diff,1},CA{t,diff,2},motile(:,:,1),tissueSz,abtnf,abtgf,DKtnf,D
Ktgf);

%epth liv to dead
disp('apoptosis/necrosis')
[epthMat]= hel2dead(CA{t,fixed,1}, CA{t,diff,1},motile,tissueSz,abapop);

%---------------------second update----------------------------------------
%epth mitosis and fibroblast healing (separate this later)
fprintf('\t\t\t\t\t healing \n')
[epthMat,motile]=  dead2hel(epthMat, motile,tissueSz,mt,td,tclg);

%mobile cells dead if life is over
disp('immune cells age')
[motile]=wbc2dead(motile);

%macrophage moves randomly or toward TNF
fprintf('\t\t\t\t\t immune cells move \n')
%inactivated
[motile]= wbcmove(motile,1,mcr_v,CA{t,diff,1},tissueSz,nrn);
%activated
[motile]= wbcmove(motile,2,mcr_v,CA{t,diff,1},tissueSz,nrn);
%reduced speed
% [motile]= wbcmove(motile,2,mcr_v-2,TNFmat,tissueSz);

%fibroblast moves randomly or toward TGF
[motile]=wbcmove(motile,11,mcr_v,CA{t,diff,2},tissueSz,nrn);

%Repopulate mobile cells every 5 ticks if cell density is below average
tpopl=tpopl-1;
if tpopl ==0
    disp('repopulation')
    tpopl=tpoplc;
%     strange=[1 10];
    [motile]=populate(motile,sval1,[1 10],nMacroph,musig);
%     strange= [11 20];
    [motile]= populate(motile,sval2,[11 20],nFibrob,musig);
end

end   %time loop

%display total computational time
cta(1)=toc;
if cta(1) < 60
tun='seconds';
tc=1;
else if cta(1)>= 60 & cta(1) < 3600
```

```
tun='minutes';
tc=60;
else if cta(1) >= 3600
tun='hours';
tc=3600;
end
end
end
fprintf('total time: %4.2f %s \n',cta(1)/tc,tun)

end  %function end
```

7.2.3 SUBROUTINE STRAINDIST (STRAIN DISTRIBUTION)

```
function [epst]= straindist(tissueSz,Amp,type)

% type=4;

if type==1 %gaussian crest 1
% A= Amp/0.0080;
% mu = [0 0]; Sigma = [20 1; 1 20]; %case 1
% A= Amp/0.0796;
% mu = [0 0]; Sigma = [2 0.1; 0.1 2]; %case 2
A= Amp/ 0.793;
mu = [0 0]; Sigma = [0.2 0.01; 0.01 0.2];
x1=linspace(-3,3,tissueSz(1));  [X1,X2] = meshgrid(x1,x1);
epst = A*mvnpdf([X1(:) X2(:)],mu,Sigma);
epst = reshape(epst,length(x1),length(x1));

elseif type==2 %sinusoidal bumps
        b=4;
        A= Amp/ b;
        x1=linspace(0,4*pi,tissueSz(1));  [X1,X2] = meshgrid(x1,x1);
        epst= A*(2+(cos(X1) + cos(X2)));
elseif type==3  %horizontal strips w/ small bumps
        b=11.9993;
        A=Amp/ b;
        x1=linspace(0,4*pi,tissueSz(1));  [X1,X2] = meshgrid(x1,x1);
        epst= A*( 5.9999 + (cos(X1) + 5*sin(X2) ) );
elseif type==4  %uniform
    epst=Amp*ones(tissueSz(1),tissueSz(2));
elseif type==5 %cos center
        b=4;
        A= Amp/ b;
        x1=linspace(0,2*pi,tissueSz(1));  [X1,X2] = meshgrid(x1,x1);
        epst= A*(2+(cos(X1) + cos(X2)));
elseif type==6 %gaussian crest 2
A= Amp/0.1590;
mu = [0 0]; Sigma = [1 0.01; 0.01 1];
x1=linspace(-3,3,tissueSz(1));  [X1,X2] = meshgrid(x1,x1);
epst = A*mvnpdf([X1(:) X2(:)],mu,Sigma);
```

```
epst = reshape(epst,length(x1),length(x1));

elseif type==7 %gradation left high to right low
        b=   20.9999;
        A= Amp/ b;
        x1=linspace(0,1*pi,tissueSz(1));  [X1,X2] = meshgrid(x1,x1);
        epst= A*((20*cos(X1) + 1*sin(X2)));

end

end
```

7.2.4 SUBROUTINE POPULATE (POPULATE THE GRID WITH MOTILE CELLS)

```
function [motile] = populate(motile,sval,strange,celldensity,musig)
%for one type of mobile cell
rng('shuffle')
ncell= length(find(motile(:,:,1) >= strange(1) & motile(:,:,1) <= strange(2)
));

%non-occupied grid
[xe,ye]= find(motile(:,:,1) == 0);
xye=[xe,ye];
necell= length(xe);
xeidx=[1:1:necell];

% if ncell < celldensity
%stochastic: mu regulates skewness toward + or -, sig: spread of tolerances
mu=musig(1); sig=musig(2);
if ncell < celldensity+ round((sig*(rand-mu))*celldensity)

%location of new cells
% randomly select element in [xe,ye] -> empty grid location
noisycd= celldensity+ round((sig*(rand-mu))*celldensity);
newidx= datasample(xeidx, noisycd ) ;
fillup=noisycd-ncell;
    for igrid=1:fillup
    motile( xe(newidx(igrid)), ye(newidx(igrid)) ,1)= sval(1);
    end
    for igrid=1:fillup
    motile(   xe(newidx(igrid)),   ye(newidx(igrid))   ,2)=   randi([sval(2)-10
sval(2)+10]);
    end
end
```

7.2.5 SUBROUTINE INACT2ACT (MACROPHAGE ACTIVATION BY STRAIN)

```
function [MacrophMat]=inact2act(MacrophMat,epthStrain,A,abia)
```

```
%1 = inactivated. 2=activated
%macrophage is activated by level of strains (directional) in connective
%tissue, in this case, macrophmat grid also contains strain information
%macrophages releases TNF (pro-inflammatory) & TGF (anti-inflammatory) by
strains
%macrophage moves toward TNF
rng('shuffle');

szmcrMat=size(MacrophMat);
[wx,wy]=find(MacrophMat==1); %find inactivated macrophages
totalMCR=length(wx);


%"constitutive" relation for macrophages activation
%based on probability distribution with some bounds, based on TNF distribution
%on literature
%exponential

for cntMCR=1:totalMCR

        if wx(cntMCR)-1>0 && wx(cntMCR)+1<szmcrMat(1) && wy(cntMCR)-1>0 &&
wy(cntMCR)+1<szmcrMat(2) %boundary detect
            %this is the 'constitutive'
%             disp('block 1 activated')
            Pac=A*random('Beta',abia(1),abia(2));
            eps=epthStrain(wx(cntMCR),wy(cntMCR));

           if Pac <= eps
%                disp('block 2 activated')
            MacrophMat(wx(cntMCR),wy(cntMCR))=2;
           end
        end
end

end
```

7.2.6 SUBROUTINE CYTODIFF (CYTOKINE DIFFUSION AND RELEASE)

```
function [TNFmat,TGFmat]=
cytodiff(TNFmat,TGFmat,motile,tissueSz,abtnf,abtgf,DKtnf,DKtgf)

%diffusion-----------------------------------------------------------------
%assume unity pseudo-diffusity constant

% nrn=10;
% TNF diffuse
szmTNF=size(TNFmat);
TNFt= TNFmat;
TGFt= TGFmat;
```

```
Dp=DKtnf(1); Kp=DKtnf(2);  %pro-inflammatory/activator ~ TNF
Da=DKtgf(1); Ka=DKtgf(2);  %anti-inflammatorty/inhibitor ~ TGF

for i=1:szmTNF(1)
    for j=1:szmTNF(2)
           [mi,mj]= mooresnei(i,j,1,tissueSz);
           grn=TNFmat(mi,mj);
           grn(2,2)=0;
           grn(1,1)=0; grn(1,3)=0; grn(3,1)=0; grn(3,3)=0;

   TNFt(i,j)   =   TNFmat(i,j)   +   Dp*(   (sum(sum(grn)))-4*TNFmat(i,j)   )   -
Kp*TNFmat(i,j);

           [mi,mj]= mooresnei(i,j,1,tissueSz);
           grn=TGFmat(mi,mj);
           grn(2,2)=0;
           grn(1,1)=0; grn(1,3)=0; grn(3,1)=0; grn(3,3)=0;

   TGFt(i,j)   =   TGFmat(i,j)   +   Da*(   (sum(sum(grn)))-4*TGFmat(i,j)   )   -
Ka*TGFmat(i,j);

    end
end
% TGFmat=round(TGFt,nrn);
% TNFmat=round(TNFt,nrn);
TGFmat=TGFt;
TNFmat=TNFt;

%release-----------------------------------------------------------------------
%activated macrophages action----------------------------------------
%macrophages release TNF: can be stochastic or per ticke
%rate of release ("per tick" mode) can be deterministic or stochastic
%probability to release, Pr:
% global totalIters
% rt=5;
% c=totalIters/rt;
% Pr=c/totalIters;
% Pr=1/rt;

szmcrMat=size(motile);
[wx,wy]=find(motile==2);
totalMCR=length(wx);

for cntMCR=1:totalMCR
%stochastic release, tuned by TGF level
   Pac=random('Beta',abtnf(1),abtnf(2));
   tgflev= TGFmat(wx(cntMCR),wy(cntMCR));
        %the more tgf, the slower tnf release
        if Pac >= tgflev
        TNFt(wx(cntMCR),wy(cntMCR))= 1;
        end

% %stochastic time
%     Pp= rand;
```

```
%     if Pp < Pr/(tgflev+1)
%     TNFmat(wx(cntMCR),wy(cntMCR))= 1;
%     end

end

%TGF release by fibroblast
szmcrMat=size(motile);
[wx,wy]=find(motile==11);
totalMCR=length(wx);
for cntMCR=1:totalMCR
   %stochastic release based on TNF level
   Pac=random('Beta',abtgf(1),abtgf(2));
   tnflev= TNFmat(wx(cntMCR),wy(cntMCR));
        %the more tnf, the higher tgf release
        if Pac <= tnflev
        TGFt(wx(cntMCR),wy(cntMCR))= 1;
        end
end

% TGFmat=round(TGFt,nrn);
% TNFmat=round(TNFt,nrn);
TGFmat=TGFt;
TNFmat=TNFt;

end
```

7.2.7 SUBROUTINE HEL2DEAD (APOPTOSIS)

```
function [epthMat]=hel2dead(epthMat,TNFmat,motile,tissueSz,abapop)
%L -> Dead
%0 -> 1
%by TNF level & collagen existent (not level)
rng('shuffle');

% tic;
for xs=1:tissueSz(1)
% tic;
for ys=1:tissueSz(2)
    %if fibrosis, keep flag 0
    if motile(xs,ys,1)~=-2
     if epthMat(xs,ys) ==0
    %damage by TNF on THE cell
     Pdead= random('Beta',abapop(1),abapop(2));
     tnflev= TNFmat(xs,ys);
     if Pdead < tnflev
         epthMat(xs,ys)=1;
     else
     %damage by collagen existent in Moore's neighborhood
     [mx,my]=mooresnei(xs,ys,1,tissueSz);
     %detect if there is collagen
     clxy= find(motile(mx,my,1)==-2);
```

```
      lclxy=length(clxy);
      %if collagen
      if lclxy > 0
        Pdead=datasample([0 1],1,'Weights',[1 1+(lclxy/9) ]); %max prob is 1/0
= 2/1
        epthMat(xs,ys)=Pdead;
      end

      end
      end
     end
end
end

end
```

7.2.8 SUBROUTINE DEAD2HEL (HEALING)

```
function [epthMat,motile]=dead2hel(epthMat,motile,tissueSz,mt,td,tclg)
%1. healing by mitosis
rng('shuffle');
%mitosis rate: mt iteration
%probability of mitosis:
Pmt=1/mt;
% K=1;
[xs,ys]=find(epthMat==1);
lenxs=length(xs);
if lenxs>0
%Method 1
% for cntrx=1:lenxs
%    [mx,my]=mooresnei(xs(cntrx),ys(cntrx),1,tissueSz);
%    dumMat=epthMat(mx,my);
%    nLive=sum(sum(dumMat==0));
%    P_cal=1-(1-rand(1)).^(nLive/( 10*(TNFmat(xs(cntrx),ys(cntrx))+1) ));
%    if P_cal>=P_dh
%        epthMat(xs(cntrx),ys(cntrx))=0;
%    end
%
% end
%Method 2
for cntrx=1:lenxs
%    Ctnf= TNFmat(xs(cntrx),ys(cntrx))+1;
%    [mx,my]=mooresnei(xs(cntrx),ys(cntrx),1,tissueSz);
%    eptmoore=epthMat(mx,my);
%    nLive=sum(sum(eptmoore==0));
   P_cal= rand;
   if P_cal < Pmt  %/(K*Ctnf)
       epthMat(xs(cntrx),ys(cntrx))=0;
   end
```

```
end
end

%2. fibroblast healing
% healing is 5 ticks and then fibroblast dissappear
[wx,wy]=find(motile(:,:,1) == 11);
motileTemp= motile;
lenxs = length(wx);
% mn=1;
% td=5;
for cntrx=1:lenxs
%epth states in Moore's neighborhood
%     [mx,my]= mooresnei(wx(cntrx),wy(cntrx),mn,tissueSz);
    [mx,my]= mooresnei(wx(cntrx),wy(cntrx),1,tissueSz);
    %if there is dead epth in vicinity, %fibroblast differentiate, not
    %moving = -1, but undetected as mobile cells--> affect collision, can
    %be fixed by modifying move rules so that >0 moves and <0 stay, so
    %find(~= 0) instead
    localdm= epthMat(mx,my)== 1;
    if sum(sum( localdm ))> 0
     %fibroblast heals & reset clock for
     %healing

        motile(wx(cntrx),wy(cntrx),1)= -1;
        motile(wx(cntrx),wy(cntrx),2)= td;

     dmidx = datasample( find(localdm== 1), 1 );
     %coordinates in column
     %make dummy moore's matrix, take element using lin idx
%      mxm= repmat(mx,[length(mx) 1]);  mym= repmat(my',[1 length(my)]);
     [mxm,mym]= mooresmatrix(mx,my);
     gx(cntrx)= mxm(dmidx); gy(cntrx)= mym(dmidx);

     %move fibroblast to randomly selected dead cell in vicinity
     motileTemp(gx(cntrx),gy(cntrx),:) = motile(wx(cntrx),wy(cntrx),:);
     motile(wx(cntrx),wy(cntrx), :)= 0;
     motile(gx(cntrx),gy(cntrx),:) = motileTemp(gx(cntrx),gy(cntrx),:);

    end
end

%3. Fibroblast heals after t ticks, and dissapear
[wx,wy]=find(motile(:,:,1) == -1);
% motileTemp= motile;
lenxs = length(wx);
% tclg= 10;
if lenxs> 0
for ifbr=1: lenxs
    if motile(wx(ifbr),wy(ifbr),2) >0
    motile(wx(ifbr),wy(ifbr),2)= motile(wx(ifbr),wy(ifbr),2) -1;
    else
%     motile(wx(ifbr),wy(ifbr),1)= 0;
    %assuming fibroblast correctly moved to dead epth above, if moved
    epthMat(wx(ifbr),wy(ifbr))= 0;
```

```
    %fibroblast deposit collagen on last place
    motile(wx(ifbr),wy(ifbr),1)= -2;
    motile(wx(ifbr),wy(ifbr),2)= tclg;
    end
end
end

%4. collagen dissolve, 10% per tick
%so collagen is on former dead epth then
[wx,wy]=find(motile(:,:,1) == -2);
lenxs = length(wx);
if lenxs> 0
for ifbr=1: lenxs
    if motile(wx(ifbr),wy(ifbr),2) >0
    motile(wx(ifbr),wy(ifbr),2)= motile(wx(ifbr),wy(ifbr),2) -1;
    else
    %collagen dissapear
    motile(wx(ifbr),wy(ifbr),1)= 0;
    end
end
end

end
```

7.2.9 SUBROUTINE WBC2DEAD (MOTILE CELLS LIFE TIME/RERANDOMIZATION)

```
function [motile]=wbc2dead(motile)

%mobile motile cells age states
%motile that stop moving don't age here
[xs,ys]=find(motile(:,:,1) > 0);
cntx=length(xs);

for igrid=1:cntx
   %if age tick is over, mobile cell dies
   if motile(xs(igrid),ys(igrid),2)== 0
    motile(xs(igrid),ys(igrid),1)= 0;
   else
   %aging
   motile(xs(igrid),ys(igrid),2) = motile(xs(igrid),ys(igrid),2) -1;
   end
end


end
```

7.2.10 SUBROUTINE WBCMOVE (MOTILE CELLS LOCOMOTION)

```
function [motile]=wbcmove(motile,ctype,gridSz,cytomat,tissueSz,nrn)
%chemotaxis
%move one type of cell
%don't collide any other mobile cells
 rng('shuffle');
[wx,wy]=find(motile(:,:,1)== ctype);
ctWBCs=length(wx);
motiletemp=motile;
%  mooreidx= 1:1:(2*gridSz+1)^2;

for igrid=1:ctWBCs
    %Moore's neighbor of a mobile cell
    [mx,my]= mooresnei(wx(igrid),wy(igrid),gridSz,tissueSz);
    [mxm,mym]= mooresmatrix(mx,my);
%     %collect all local unoccupied grid
%     xye= find(motile(mx,my,1)== 0);
%     lxye=length(xye);

    %collect all local unoccupied grid
    xyu=find(motile(mx,my,1)== 0);

    %collect all local occupied grid, if exist
    xye= find(motile(mx,my,1)~= 0);
    lxye=length(xye);
    %if there exist space to move
    if lxye <= (2*gridSz+1)^2
    %prepare the weight matrix
    %local cytokine level
    locyto=round(cytomat(mx,my),nrn);
         %if no TNF, then uniform probability
            if sum(abs(locyto))==0 locyto(:,:)=1;
            end

    %quick fix for negative concentration:
    locyto(locyto<0)=0;

    %"don't move to occupied" - quick fix
    locyto(xye)=0;

    % "don't stay" - quick fix
    locyto(2,2)=0;

    moveWeights= reshape(locyto,[(2*gridSz+1)^2 1]);
        %if no TNF on unccopied grid, then uniform probability on
        %unoccupied
            if sum(abs(moveWeights))==0 moveWeights(xyu)=1;
            end

%   moveWeights= locyto(xye);
    lmw=length(moveWeights); %lmw should be = lyxye though, check again
%     moveWeights= reshape(locyto(xye),[],1);
```

```
    newidx = datasample([1:1:lmw],1,'Weights',moveWeights');

    gx(igrid) =  mxm(newidx);  gy(igrid) =  mym(newidx);
    %else if there is not space to move-----------------------------

    else
% disp('stay------------------------------------------------------------------
---------')
    %stay, don't need to execute above lines
     gx(igrid) = wx(igrid);  gy(igrid) = wy(igrid);
    end
end

%move the mobile cells (and its properties; state, age)
for igrid=1:ctWBCs
    motiletemp( gx(igrid), gy(igrid) ,:) = motile( wx(igrid),wy(igrid) ,:) ;
    motile(wx(igrid),wy(igrid) ,:)= 0 ;
    motile( gx(igrid), gy(igrid) ,:) =  motiletemp( gx(igrid), gy(igrid) ,:) ;
end

end
```

APPENDIX B

SUPPLEMENTAL MATERIALS FOR CHAPTER 3

COMPUTATIONAL SIMULATION OF CELL-TO-CELL COMMUNICATION DURING INFLAMMATION AND AGING

8.1 PSEUDOCODE

8.1.1 TRANSFER ENTROPY

```
Begin
    Import pairs of temporal data: $X(t)$ and $Y(t)$
    Binning of $\{X(\mathrm{t}), X(t-1), Y(t-1)\}$ ( estimation of $p(X,Y,Z)$ )
    Calculate Eq. 3.8 ( estimation of $p(Y(t-1)$ )
    Calculate Eq. 3.9 ( estimation of $p(X(t),\ Y(t-1)$ )
    Calculate Eq. 3.10 ( estimation of $p(X(t-1),\ Y(t-1)$ )
    Calculate Eq. 3.7 (estimation of $T_{X\to Y}$)
End
```

8.1.2 TRANSFER ENTROPY NETWORK

```
Begin
    Initiate network nodes $X_i$ and $Y_i$
    Import $T_{X\to Y}$ matrix
```

```
    For i=1 to length($T_{X \to Y}(:,j)$)
      For j=1 to length($T_{X \to Y}(i,:)$)
        If $\frac{T_{X \to Y}(i,j)}{T_{X \to Y}(j,i)} < 1$ or $Tc$ (ratio of transfer entropy $X_i \to Y_i$ and $Y_i \to X_i$)
          $Y_i \to X_i$ (create a network edge from $Y_i$ to $X_i$)
        Else
          $X_i \to Y_i$  (create a network edge from $X_i$ to $Y_i$)
        End
      End
    End
End
```